

AN ADIABATIC DEMAGNETIZATION APPARATUS
FOR NUCLEAR ORIENTATION

by

ROBERT LLOYD ALBERT GORLING

B.A., University of British Columbia, 1966

A THESIS SUBMITTED IN PARTIAL FULFILMENT OF
THE REQUIREMENTS FOR THE DEGREE OF

MASTER OF SCIENCE

in the Department

of

Physics

We accept this thesis as conforming to the
required standard

THE UNIVERSITY OF BRITISH COLUMBIA

April, 1970

In presenting this thesis in partial fulfilment of the requirements for an advanced degree at the University of British Columbia, I agree that the Library shall make it freely available for reference and study.

I further agree that permission for extensive copying of this thesis for scholarly purposes may be granted by the Head of my Department or by his representatives. It is understood that copying or publication of this thesis for financial gain shall not be allowed without my written permission.

Department of Physics

The University of British Columbia
Vancouver 8, Canada

Date April 15, 1970

ABSTRACT

A cryostat has been built for cooling specimens to temperatures of the order of a hundredth of a Kelvin by thermal contact with an adiabatically demagnetized paramagnetic salt pill. The apparatus was designed for performing nuclear orientation experiments. This thesis describes the construction of the apparatus and experimental tests studying the nuclear orientation of ^{60}Co in an iron plate.

The paramagnetic salt used was chromium potassium alum in an alum-glycerine slurry. In addition to the chrome alum pill a guard pill of manganous ammonium sulphate was used between the alum pill and the 1K helium bath. The pills were supported and thermally isolated by German silver spacers. A copper heat link was embedded in the alum-glycerine slurry and soldered to the specimen to provide thermal contact. Several heat links were used ranging from a bundle of five thousand copper wires to a copper foil "concertina" arrangement. A Ventron niobium-titanium superconducting solenoid which produced fields up to 48 kilogauss was used for the magnetic cooling. A superconducting polarizing solenoid was used to magnetically saturate the polycrystalline iron plate.

Anisotropies in the gamma radiation intensity from ^{60}Co of 7 to 11 per cent corresponding to temperatures of 37 to 45 m K were observed.

TABLE OF CONTENTS

	Page
ABSTRACT	ii
LIST OF TABLES	vi
LIST OF FIGURES	vii
 CHAPTER I INTRODUCTION	
1.1 Anisotropy of Radiation from Oriented Nuclei	1
1.2 Static Nuclear Orientation	3
1.3 Experimental Nuclear Orientation	4
i) Low Temperature	4
ii) The Macroscopic Axis	5
iii) Thermometry	5
iv) The Experiments	5
1.4 Contact Cooling	5
1.5 The Hyperfine Field and the Effective Field	6
1.6 Mechanisms for Hyperfine Fields in Metals	9
i) Exchange Polarization	9
ii) Transferred Hyperfine Structure	10
iii) RKKY	12
1.7 Other Experimental Techniques	13
i) NMR	13
ii) Resonant Destruction of Nuclear Orientation (NMR-ON)	14
iii) Mossbauer Effect	14
iv) Perturbed Angular Correlations	14
v) Nuclear Specific Heat	14
 CHAPTER II THE LOW TEMPERATURE APPARATUS	
2.1 The Outer Cryostat	16

CHAPTER II (continued)

i)	The Glass Dewars	16
ii)	Liquid Nitrogen Filler	17
iii)	Liquid Helium Transfer	17
iv)	Boil-Off Rate	19
2.2	The Demagnetization and the Remnant Field.	19
i)	The Solenoid	19
ii)	The Remnant Field	20
iii)	NMR Field Measurement of Demagnetization	21
	Solenoid	
2.3	The Polarizing Solenoid	21
2.4	Magnetic Saturation of Specimen	23
2.5	The Inner Cryostat	25
i)	Description	25
ii)	The 1K Helium Bath	25
iii)	Solder Joins in Inner Cryostat	25
2.6	The Vacuum Requirements and Low Temperature	29
	Vacuum Techniques	
i)	The Inner and Outer Jackets	29
ii)	Other Pumping Requirements	30
2.7	The Paramagnetic Salt Assembly	30
i)	Chrome Potassium Alum Pill	30
ii)	The Guard Pill	31
iii)	The Spacers	31
2.8	The Heat Link and the Specimen Temperature	31
2.9	Vibrations	35
2.10	Experimental Procedure	36

CHAPTER III NUCLEAR ORIENTATION OF ^{60}Co IN IRON

3.1	The Temperature Dependence of the Anisotropy of ^{60}Co	40
-----	--	----

	Page
CHAPTER III (continued)	
3.2 The Preparation of the Source	42
3.3 The Detectors and Electronic Circuitry	42
3.4 The Experiments: Data and Results	44
i) The Raw Data	44
ii) Corrections to the Raw Data	46
iii) The Results	48
CHAPTER IV FUTURE MODIFICATIONS OF THE APPARATUS	
4.1 Low Temperature	61
i) Heat Leaks to the Demagnetized System	61
ii) The Remnant Field	62
iii) The 1K Helium Bath	62
iv) Liquid Helium Loss	62
4.2 Resonant Destruction of Nuclear Orientation	62
4.3 Detectors	63
i) Ge(Li) Detectors	63
ii) Si(Li) Detectors	63
REFERENCES	64

LIST OF TABLES

Table		Page
2.1	NMR Field Calibration	22
2.2	Typical Low Temperature Run	38
3.1	The ⁶⁰ Co Runs	49

LIST OF FIGURES

Figure		Page
2.1	The Outer Cryostat (Schematic)	17
2.2	Saturation of Iron Foil	24
2.3	Saturation of Specimen (<u>In Situ</u> Experiment).	26
2.4	Inner Cryostat and Demagnetization Assembly	28
2.5	The Spacers	32
2.6	The Specimen Temperature	34
3.1	The Decay Scheme of ^{60}Co	41
3.2	The ^{60}Co Thermometer	43
3.3	The Gamma Radiation Detection Apparatus (Schematic)	45
3.4	Run 1	54
3.5	Run 2	55
3.6	Run 3 - An Uninterrupted Run	56
3.7	Runs 4 and 5	57
3.8	Run 6	58
3.9	Run 7	59

ACKNOWLEDGEMENTS

I wish to thank Dr. B. G. Turrell for his constant encouragement and assistance throughout this work.

Of the many members of the Physics Department who have contributed technical assistance to the work, I especially want to thank Mr. John Lees and Mr. E. P. Williams who built and maintained the glassware.

CHAPTER I

INTRODUCTION

In this chapter some of the basic theory and procedures will be introduced. The spatial anisotropy of gamma radiation from a system of oriented nuclei is discussed in terms of certain orientation parameters. The mechanisms of static nuclear orientation are briefly presented in terms of a hyperfine Hamiltonian. The electronic contributions to magnetic hyperfine interactions will be briefly introduced with an emphasis on dilute impurities in ferromagnetic metals. The technique of nuclear orientation including a discussion of contact cooling is given. In addition a brief discussion of some of the other techniques used in the study of hyperfine fields is presented.

1.1 Anisotropy of Radiation from Oriented Nuclei

Given a system of nuclei of spin I and magnetic moment μ , a magnetic field H will split the ground state into $2I + 1$ sub-levels equally spaced in energy by $\mu H/I$. In thermal equilibrium the population of these levels is given by the Boltzman distribution. For the M th level, where $-I < M < I$, the normalized occupation is

$$a_M = a_o \exp (E_M/kT)$$

where E_M is the energy of the M th sub-level and a_o is the normalization constant. For the magnetic interaction above the occupation is

$$a_M = a_o \exp (-\mu HM/IkT)$$

It is common in angular correlation work to describe the relevant

properties of the nucleus by an irreducible tensor T_{qk}^1 . For problems of cylindrical symmetry it is only the terms

$$T_{q0} = P_q \left(M / [I(I+1)]^{\frac{1}{2}} \right)$$

which are involved. In this expression P_q is the Legendre polynomial.

The first three terms have simple physical meaning. Explicitly they are:

$$T_{00} = 1, T_{10} = M / [I(I+1)]^{\frac{1}{2}}; T_{20} = [3M^2 - I(I+1)] / 2I(I+1)$$

The first term is isotropic and is set equal to one for normalization.

The second term expresses what is called the "polarization" of the nucleus in the direction of quantization. The third term expresses the "alignment".

The orientation of the entire system of nuclei in a bulk sample of material is given by the expectation values $\langle T_{q0} \rangle$, suitably normalized. The notation used throughout this work is that of Gray and Satchler² who define the orientation parameter

$$B_{\nu} = \sum_M (2\nu + 1)^{\frac{1}{2}} C(I \nu I; M 0) a_M,$$

where C is the Clebsh-Gordon coefficient. The parameter has been tabulated for some important Hamiltonians by Blin-Stoyle and Grace³. If the nuclei in this system emit nuclear radiation decaying to a new state (of definite angular momentum) then angular momentum must be conserved. The expression for the transition probability for gamma radiation reduces to

$$W(\Theta) = \sum_{\substack{\nu \leq 2I, 2L \\ \nu \text{ even}}} B_{\nu} U_{\nu} F_{\nu} P_{\nu} \cos(\Theta)$$

This expression gives the normalized intensity of the gamma radiation as a function of the angle Θ from the quantization axis. In this expression the U_{ν} factors express the re-orientation effect of any unobserved

transitions from the initial state preceding the observed gamma decay. The F_{ν} factors refer to the observed transition. These two factors U_{ν} and F_{ν} are functions of the preceding and final states of the transition and the angular momentum of the radiation. "L" is the highest multipole component of the observed transition. For observed transitions not conserving parity-beta radiation - the requirement that ν be even is dropped. A full discussion of this scheme including the form of F_{ν} and U_{ν} is given in reference 4.

A useful experimental parameter is the anisotropy, ϵ , given by,

$$\epsilon = \frac{W(90^\circ) - W(0^\circ)}{W(90^\circ)}$$

1.2 Static Nuclear Orientation

Only at temperatures where the splitting of the nuclear sub-levels is comparable to the thermal energy, that is,

$$E_M - E_{M+1} \approx kT,$$

is appreciable nuclear orientation achieved. For a typical magnetic interaction ($\mu \approx 1$ n.m., $I \approx 1$) this requires a temperature of the order of a hundredth of a degree and a field of the order of a hundred kilo-oersted. In general other hyperfine interactions can be involved. A phenomenological spin Hamiltonian⁵ in an external field is,

$$\begin{aligned} \mathcal{H} = & \underline{\mu} \cdot \underline{H} + \mu_0 [g_{11} H_z S_z + g_{\perp} (H_x S_x + H_y S_y)] \\ & + [A S_z I_z + B (S_x I_x + S_y I_y)] \\ & + [D S_z^2 - 1/3 S(S+1)] + [P \{ I_z^2 - 1/3 I(I+1) \}] \end{aligned}$$

where \underline{S} is the effective spin determined by the multiplicity of the low lying electronic energy levels.

The first term in the Hamiltonian gives the "brute force" method of achieving nuclear orientation. It requires the application of an external field typically 10^5 to 10^6 oersted. The terms in g_{\parallel} and g_{\perp} are Zeeman electronic terms which orient the effective spin in an external field. For a ferromagnet the "external field" H will include the Lorentz field of the electronic dipole moments.

In the Gorter-Rose method of nuclear orientation, the polarization of the effective spin by the Zeeman interaction will produce orientation of the nuclear spin by the hyperfine terms in A and B. If A dominates B then the nucleus aligns along the effective spin; if B dominates then the nucleus aligns perpendicular to the effective spin. The term in D represents the electronic interaction with the crystalline electric field and can also produce nuclear orientation through the hyperfine terms in A and B (provided $S > \frac{1}{2}$). This is the Bleaney method. It is also feasible to produce nuclear orientation through the interaction of the nuclear quadrupole moment and the electric field gradient as given in the P term.

1.3 Experimental Nuclear Orientation

The actual apparatus used in this work is very briefly introduced in this section.

i) Low Temperature The low temperature is produced by adiabatic demagnetization of a chrome potassium alum slurry. Magnetic fields up to 48 kilo-oersted were produced in a superconducting solenoid. When the alum is adiabatically demagnetized from 20 k oe. per degree it cools to $.012^{\circ}\text{K}$. At this temperature there is a magnetic ordering transition with a large specific heat anomaly. A copper heat link embedded in the salt and soldered to the source provides the thermal contact between the salt and the radioactive specimen.

ii) The Macroscopic Axis To observe macroscopic effects of nuclear orientation an axis of quantization must be defined. Since the fields which orient the nuclei are electronic in origin it is necessary to align the electronic spins. In this experiment they are aligned by the exchange field of the iron. Thus the polycrystalline iron foil is magnetically saturated by a superconducting solenoid to remove the domains.

iii) Thermometry The most suitable method of thermometry is the observation of the anisotropy of gamma radiation of aligned nuclei for which all the orientation and decay scheme parameters are known. ^{60}Co is used in this experiment because it has been well studied both for nuclear and hyperfine parameters, and also because it has a relatively high anisotropy at temperatures of approximately .01 K.

iv) The Experiments After demagnetization, the count rates at 0° and 90° to the axis of quantization were observed. The count rates were normalized to the isotropic rates observed at helium bath temperatures.

1.4 Contact Cooling

There are three distinct thermal barriers giving temperature gradients between the source and the pill. First, the heat must be conducted across the alum-copper interface. The heat is conducted across by phonons. Little⁶ has given the theoretical formula,

$$\dot{Q} = k A (T_1^4 - T_2^4)$$

where A is the contact surface area. The value of the constant k seems to vary with the experimental set-up. The best value obtained experimentally⁷ is,

$$k \doteq 7.5 \times 10^4 \text{ erg sec}^{-1} (k)^{-4} \text{ cm}^{-2}.$$

The conductivity of the copper is due primarily to the conduction electrons. Hence, the heat must be transferred from conduction electrons to phonons. Little has shown for this barrier that,

$$\dot{Q} = 1.0 \times 10^{10} (T_1^5 - T_2^5) \text{ erg sec}^{-1} \text{ cm}^{-3},$$

where the rate is given per unit volume. The volume over which the transfer can take place is given by the mean free path of the phonons, $L = 4.0 \times 10^{-3} (T^{-1}) \text{ cm}$.

The third thermal barrier arises simply from the conductivity of the copper:

$$\dot{Q} = k (T_1 - T_2) A L^{-1}$$

where $k = 1.0 \times 10^7 (T) \text{ erg sec}^{-1} \text{ K}^{-1}$.

The actual experimental considerations and calculation of the source temperature as a function of the heat input is given in Chapter II.

1.5 The Hyperfine Field and the Effective Field

The magnetic interaction Hamiltonian for an electron of orbital angular momentum $\underline{\ell}$, spin angular momentum \underline{s} , with a nucleus of spin \underline{I} is given by

$$\begin{aligned} \mathcal{H} = & \frac{\mu_0}{4\pi} 2\beta \left(\frac{\mu_I}{I} \right) \{ [\underline{\ell} \cdot \underline{I} \langle r^{-3} \rangle] \\ & + [\underline{s} \cdot \underline{I} - 3 (\underline{s} \cdot \underline{r}_0)(\underline{r}_0 \cdot \underline{I})] \langle r^{-3} \rangle \\ & + [\underline{I} \cdot \underline{s} \delta(r) \langle r^{-3} \rangle] \} \end{aligned}$$

Here, β is the Bohr magneton and \underline{r}_0 is the unit vector between the nucleus

and electron. The first term in the sum is the orbital contribution; the second is the dipolar interaction between the spins of the electron and nucleus; the third is the Fermi contact term. The Fermi contact term represents the interaction of the nucleus with that electron that has a finite probability of being at the nuclear site. The first two terms are both zero for S-state ($l = 0$) electrons. The contact term is non-zero for, and only for, S-state electrons. It is convenient to think of the interaction in the form of a magnetic field of the electron at the nucleus as follows,

$$\mathcal{H} = \underline{\mu}_I \cdot \underline{H}_{h.f.}$$

If the interaction is diagonal in $\underline{H}_{h.f.}$ and \underline{I} , the nuclear energy levels are given by

$$E_M = \langle \underline{H}_{h.f.} \rangle M \frac{\mu_I}{I}$$

The three terms in the Hamiltonian each give rise to a magnetic field; the total field is their vector sum.

The orbital field, for L-S coupling is,

$$H_L = \frac{\mu_0}{4\pi} 2\beta \langle L \rangle \langle r^{-3} \rangle$$

In the 3d transition metals the orbital angular momentum is nearly quenched ($\langle L \rangle = 0$) by the crystalline electric field so that this contribution is small. From the relations

$$\underline{L} + \underline{S} = \underline{J}; \quad \underline{L} + 2\underline{S} = g\underline{J}$$

we have $\underline{L} \approx -(g - 2)\underline{S}$. Hence,

$$H_L = \frac{\mu_0}{4\pi} 2\beta (g - 2) \langle S \rangle \langle r^{-3} \rangle,$$

for 3d transition metals. For rare earth metals the spin-orbit coupling

is dominant. Hence, the orbital hyperfine field from the 4f electrons is the dominant contribution.

The spin-dipolar field is (in L-S coupling)

$$H_D = \frac{\mu_0}{4\pi} g_s \beta \langle S \rangle \langle r^{-3} \rangle \langle 1 - 3 \cos^2 \Theta \rangle.$$

The angle Θ is taken between the vector giving the nuclear spin and the position vector giving a small volume element of electronic spin. The averages in Θ and r are taken over the electron orbit; the average in S is an ensemble average over the occupied spin states.

The contact field is given by

$$H_s = \frac{\mu_0}{4\pi} 2 \beta \langle S \rangle \langle r^{-3} \rangle$$

provided, however, that $\langle r^{-3} \rangle$ is the same for all the spin states averaged in the factor $\langle S \rangle$. Large hyperfine fields can result if $\langle r^{-3} \rangle$ is not the same for both spins in an S-state orbital. H_s can be written in a form which clearly shows the non-zero value of the S-state wavefunction at the nuclear site (in c.g.s. units):

$$H_s = \frac{8\pi}{3} 2 \beta s |\Psi(0)|^2,$$

for one S electron.

The hyperfine field which has been discussed is not measured directly, What is measured is the effective field given by

$$H_{\text{eff}} = H_{\text{h.f.}} + H_L + H_0 - DM.$$

$H_{\text{h.f.}}$ is the hyperfine field, H_L is the Lorentz field of the magnetic dipoles surrounding the "atomic site". H_0 is the externally applied field and DM is the demagnetizing field of the surface "magnetic poles" in terms of a demagnetizing (geometrical) factor and the magnetization of

the sample. Notice that the sign of $H_{h.f.}$ can be determined by varying the magnitude of H_0 and noting if H_{eff} increases or decreases.

1.6 Mechanisms for Hyperfine Fields in Metals

This section will give mechanisms whereby hyperfine fields arise in metals and particularly at an impurity site in a metal.

i) Exchange Polarization Conventional Hartree-Fock calculations ignored the difference in spin up and spin down states in calculating the wave functions. Hence all states equally populated with spin up and down (such as core S-states) give zero hyperfine field in this scheme. "Spin-polarized" (unrestricted) calculations consider the exchange interaction between unpaired electrons and core "closed shell" electrons. A simple but physically meaningful model has been given⁸ which explains the results.

The exchange is found to act as an attractive force between parallel spins. For example, in a ferromagnetic metal the unpaired 3d spin up electrons attract the core S electrons of the same spin outwards towards the high density of 3d electrons. The effect is to produce a difference in the $\langle r^{-3} \rangle$, or $|\Psi_{(o)}|^2$, values of the spin states. A net hyperfine field from the Fermi contact term results:

$$H_c = \frac{8\pi}{3} 2\beta_s (|\Psi_{\uparrow(o)}|^2 - |\Psi_{\downarrow(o)}|^2)$$

Freeman and Walson have shown that this field could be -5×10^5 oersted in metallic iron (out of a total field of -3.3×10^5 oersted. This effect is called core "polarization". The 4s conduction electron contribution would be of opposite sign; the conduction electrons of spin up are pulled inwards because they lie primarily outside the 3d spins. The 4s electrons of spin up are lowered in energy, hence, the spin up band will fill with

more electrons up to the Fermi level than the spin down band. This produces a net spin up contribution-conduction electron polarization - in the 4s band. Because the spin up electrons are pulled inwards by the up spins, a net spin down polarization is left near the cell boundary (in spite of the net spin up polarization). Indeed, positron annihilation experiments in iron and nickel have measured such a net spin down⁹. A better analysis of the conduction electron problem is given by the Ruderman-Kittel-Kasuya-Yosida approach presented below. The effects will be seen to be much less "predictable" than given by the simple model.

Friedel and Daniels have proposed a model for the hyperfine fields on period V elements from silver to iodine as dilute impurities in a 3d transition metal¹⁰. The model uses the conduction electron effects discussed above. If a normally diamagnetic atom is placed substitutionally in an iron lattice (for example), provided the electrostatic perturbation in the lattice is small enough, the impurity will "see" the negative spin polarization of the outer region of the iron atoms. A negative hyperfine field will result (from the contact interaction). However, if the atom has a large electrostatic interaction, compared to the iron, with the conduction electrons the nucleus will see the net spin of the conduction band. Since this is spin-up, a positive field will result.

ii) Transferred Hyperfine Structure Polarization of electrons on an impurity atom can occur from transferred hyperfine interaction. In addition, the field on the host can be affected. Two mechanisms can account for this polarization: the "Pauli distortion effect" or admixture, and covalent bonding. These effects have been used to qualitatively explain transferred hyperfine structure on ligands in dielectric solids such as MnF_2 and KMnF_3 ⁸.

The free atom core electronic states of the solute are not in general orthogonal to the ferromagnetic electron states of the host for the same spin states. If ϕ_{\uparrow} is an orbital appropriate to the ferromagnet, and χ_{\uparrow} , χ_{\downarrow} are appropriate to the core of the solute, they will have an overlap integral $S \neq 0$ between them. These wavefunctions can be Schmidt orthogonalized obtaining the set

$$(1 - s^2)^{-\frac{1}{2}} [\phi_{\uparrow} - s\chi_{\uparrow}]; \chi_{\uparrow}; \chi_{\downarrow}$$

or the equivalent set

$$\phi_{\uparrow}; \chi_{\downarrow}; (1 - s^2)^{-\frac{1}{2}} [\chi_{\uparrow} - s\phi_{\uparrow}].$$

The free atom states of spin up on both the host (near neighbours to the impurity) and the solute are "strengthened". The impurity nucleus will see a net spin up polarization of core electrons giving a positive field. Because the host ferromagnetic wavefunction is strengthened, the host core polarization will increase giving a positive field. Because the host ferromagnetic wavefunction is strengthened, the host core polarization will increase giving a larger negative contribution to its hyperfine field.

There is an additional binding energy for the electrons if they are shared (molecular orbitals) by neighbouring atoms. Pauli exclusion prevents filled states sharing electrons, hence, to first order, only ϕ_{\uparrow} and χ_{\downarrow} can mix. The new set of wavefunctions is

$$(1 - s)^{-\frac{1}{2}} [\phi_{\uparrow} - s\chi_{\uparrow}]; \chi_{\uparrow};$$

$$(1 - 2S\gamma + \gamma^2)^{-\frac{1}{2}} [\chi_{\downarrow} + \gamma\phi_{\downarrow}].$$

This mixing corresponds to having the core spin down electron spend time in the ferromagnetic atom spin down state. γ is the weighting or "covalent" mixing factor. The effect on the impurity is to reduce the

net spin down giving a positive field (in addition to the positive admixture field). On the host the ferromagnetic spin is reduced, reducing the core polarization and the field.

Admixture and covalent bonding must both be considered in the wavefunctions for the conduction band and the ferromagnetic band in the pure metal. The two mechanisms are of opposite sign in the core polarization. The net effect on the hyperfine field is not known but it could be as large as the direct contribution to the field by the conduction electrons through the contact term.

D. A. Shirley et al. have recently suggested that transferred hyperfine structure could be the dominant effect for iodine and xenon impurities in 3d transition metals¹¹. Furthermore, it has been suggested from studies of systematics of hyperfine fields in impurities in 3d transition ferromagnetics that the core polarization is positive and constant (in a given host) across a period¹². Transferred hyperfine interaction would possibly contribute to such a mechanism.

iii) RKKY The Ruderman-Kittel-Kasuya-Yosida (RKKY) interaction refers to the effect of a local magnetic moment on the conduction electron spin distribution. The net effect on the conduction band is to lower the energy of the spin states parallel to the local moment. However, the "local" effect can be of either sign and practically any magnitude. In fact, the spin density oscillates. Indeed, calculations have shown that the net local induced spin density (as would be seen by neutron diffraction) can be 180° out of phase with the s character of the spin density at that point (as would be seen by a nucleus at the point)¹³. The calculations were done for iron and gadolinium. Such results illustrate the complexity of the conduction electron problem as well as the great progress

presently being made by theorists.

1.7 Other Experimental Techniques

In this section some of the other experimental methods used to determine hyperfine fields will be compared to nuclear orientation.

i) NMR Nuclear magnetic resonance (NMR) measures the hyperfine field directly ($h\nu = gH I$). Furthermore, because of the accuracy to which the frequency can be measured accurate determination of the field is possible. However, the ferromagnetic nuclear magnetic resonances are generally very broad and pulsed techniques are usually used. Very dilute impurities cannot be studied directly because of the weakness of the signal. Very fine powders with particle size less than the radio frequency skin depth are usually required. NMR measures the hyperfine field in the domain walls unless the specimen is magnetically saturated or strong radio frequency pulses are used.

ii) Resonant Destruction of Nuclear Orientation (NMR-ON)
Mathias¹⁸ has performed an experiment using the destruction of nuclear orientation to detect nuclear magnetic resonance. A small radio frequency (r.f.) signal coil is set up in the demagnetization chamber around the specimen source, oriented so the r.f. is perpendicular to the polarizing field. The r.f. power output of the coil must be kept small to prevent excessive heating of the source.

The resonant detection method has several advantages. The accuracy of measurement is much higher - approaching that of normal NMR. Furthermore, the hyperfine field is determined directly ($\omega = \gamma_N H_{\text{eff}}$) removing the requirement of accurate thermometry. Changing the magnitude of the polarizing field allows determination of the sign of the hyperfine field

because of the high precision. Furthermore, complete saturation of domains is not required. This is very useful in rare earth metals and cobalt. Indeed, the method has been shown to be just as applicable to non-ferromagnetic metals in spite of the loss of the r.f. enhancement.

The NMR-ON signal contains a fine structure consisting of k maxima if the statistical orientation tensor is of rank k . This feature has useful applications.

iii) Mossbauer Effect Mossbauer effect (recoilless absorption of gamma radiation) has been used to study the hyperfine interactions on a limited number of "Mossbauer nuclei" (which includes ^{57}Fe) in various electronic environments. Indeed, the "isomer shift" has been very useful in determining the amount of s-character in the orbital hyperfine field.

iv) Perturbed Angular Correlations Perturbed angular correlations measure the hyperfine field on an intermediate state of a nuclear decay. It requires sufficiently long-lived states that significant rotation of the spatial anisotropy of radiation occurs. Coincidence counting necessitates long counting times. PAC has been combined with NMR.

v) Nuclear Specific Heat

At high temperatures the population distribution of the nuclear spin levels will be uniform, that is, random orientation, but at low temperatures those spin states having lower energy will be preferred. This redistribution of the nuclear spin states gives rise to a large contribution C_N to the specific heat (Schottky anomaly) in the temperature region where it is significant. C_N has a maximum for $kT \approx \mu_I H_{\text{eff}}/I$ and is proportioned to $1/T^2$ at the high temperature end ($T \lesssim 1\text{K}$). Hence

a low temperature apparatus is required. Helium three cryostats are most frequently used but demagnetization and helium four cryostats are also used. Other contributions to the total specific heat (electronic, lattice and spin wave) have different temperature dependence and become small at low temperature so that C_N can be separated and hence H_{eff} can be determined. Small impurity contributions can give significant effects if they affect the magnetic state (for example, by the formation of local moments). High purity specimens are required unless such effects are being studied.

Besides supplementing and complementing information obtained by other methods specific heat measurements can provide a reliable estimate of, say, the position of the NMR signal which can give more accurate results.

CHAPTER II

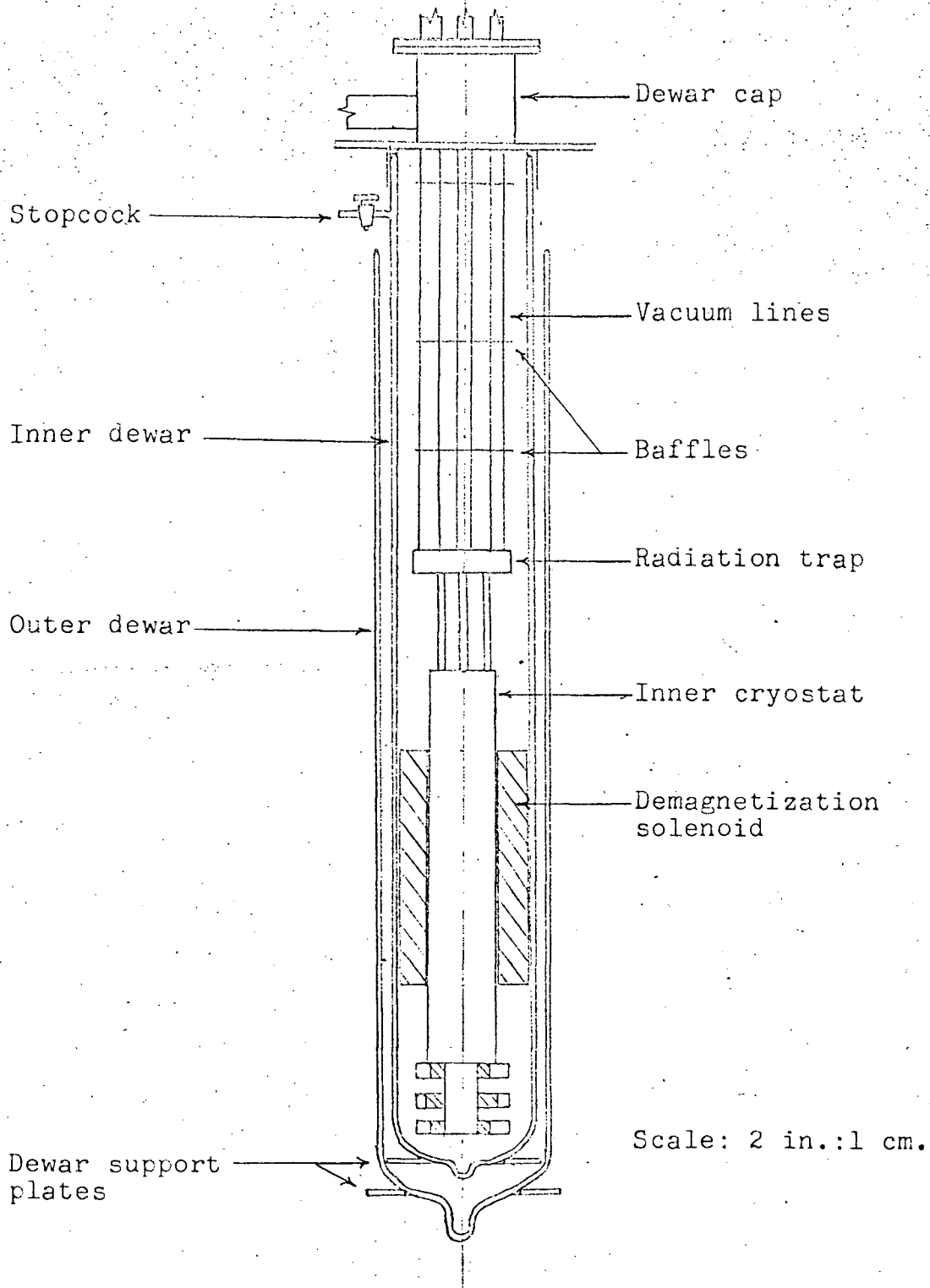
THE LOW TEMPERATURE APPARATUS

This chapter is concerned with the design, construction and operation of the low temperature apparatus used in these experiments. The first section deals with the outer cryostat which refers to the part of the machine producing liquid helium temperature (4 K). This involves the outer dewars, liquid helium transfer and the superconducting solenoids (and their power supplies). An inner cryostat allows the production of temperatures below 4 K by pumping on liquid helium. The paramagnetic salt pills used for the demagnetization and the specimen source are contained in the inner cryostat. Heat leaks to the demagnetized system are discussed as well as the actual contact cooling of the source. An experiment to determine the field of the demagnetization solenoid by NMR, and a check of the saturation of the source are given. A typical low temperature run is presented. Also mentioned in the chapter are some of the problems encountered using the apparatus.

2.1 The Outer Cryostat

The outer cryostat consisted of glass liquid nitrogen and helium dewars. Contained in the outer cryostat were the demagnetization and polarizing solenoids, the inner cryostat and pumping and electrical lines. The outer cryostat is shown in Fig. 2.1.

i) The Glass Dewars a) The liquid nitrogen, or outer dewar was a glass dewar sealed with a 'hard' vacuum in the interspace. It was supplied with a vertical slit in the silvering so the liquid level could be determined.



The Outer Cryostat (Schematic)

FIGURE 2.1

b) The liquid helium dewar, or inner dewar, was supplied with a stopcock to the interspace. A glass dewar is somewhat porous to helium gas and will become "soft" after exposure. To remove traces of helium gas in the interspace the dewar is flushed with air or nitrogen gas. The inner dewar is left with a soft vacuum of air or nitrogen to enable efficient precooling to liquid nitrogen temperatures. The gas in the interspace freezes out upon initial transfer of liquid helium leaving a "hard" vacuum. The inner dewar was supplied with a viewing slit to determine the liquid level. The inner dewar space was equipped with a safety pressure-release valve to prevent pressure build-up from helium boil-off, especially after the quenching of the superconducting solenoids.

ii) Liquid Nitrogen Filler Because the salt pill was made with a glycerine base it was necessary to keep it cold (frozen solid) at all times to prevent dehydration of the salt. This required that liquid nitrogen be maintained in the outer dewar between runs. An automatic filling device was used for this purpose.

iii) Liquid Helium Transfer It is essential that efficient use of the cold effluent helium gas be made to precool the system during a liquid helium transfer. This requires that the liquid must be delivered to the bottom of the dewar where it boils off. The effluent gas then cools the magnets and the inner cryostat as it rises. An extension on the helium transfer syphon to the bottom of the inner dewar was used. However, it was found that if the entire transfer syphon and extension were left in place after the transfer with the outside end of the syphon closed off thermal oscillations were set up in the liquid. These oscillations quickly boiled off the liquid helium. The problem was solved by leaving

the extension permanently inside the dewar with a bayonet-fitting into which the transfer syphon was inserted.

The actual transfer was performed using a pressure head of about 3 cm. of mercury pressure. After precooling the system to liquid nitrogen temperature the initial transfer took about an hour to complete and used approximately twelve litres of liquid helium. Three to five litres were used in retransferring into the cold system.

iv) Boil-Off Rate The boil-off of liquid helium was about 200 cc. per hour initially. As the level fell the rate lowered. The liquid remained above the demagnetization solenoid for about five hours allowing one or two counting runs before the liquid was "topped up".

2.2 The Demagnetization Solenoid and the Remnant Field

i) The Solenoid The demagnetization solenoid was supplied by Ventron Instruments, Magnion Division (Burlington, Mass.). The inside diameter was 2 in., the outer diameter was 4 in. and the active winding length was 7 in. It was wound with niobium-titanium wire and supplied a field of 50 kilo-oersted from a current of 62 amperes. For normal operation a current of about 55 amperes was used providing a field of 45 kilo-oersted. A persistent heat-switch was supplied with the solenoid allowing operation for long periods of time without energy loss. The solenoid's power supply was equipped to automatically shut off if the magnet "quenched" (went normal). The quench facility prevented excessive heating of the solenoid and liquid helium both. In the case of a quench the energy stored in the magnetic field was partially dissipated in a diode connected across the solenoid leads outside the cryostat.

The high current leads to the solenoid were wrapped around the pump-

ing lines for efficient cooling. They were tapered down in size from "B and S" size number 10 at the top of the cryostat to number 18 at the solenoid.

ii) The Remnant Field When a superconducting magnet is first magnetized and then demagnetized so-called persistent currents flow in the solenoid. These currents give rise to a residual or remnant field¹⁵. The remnant field must be small for efficient cooling of the paramagnetic salts. It can be readily shown that if the applied field is H_0 at initial temperature T_0 and the final field in the sample including any effective "interaction field" is H_f then the final temperature, T_f , in the adiabatic demagnetization is given by $H_f/H_0 = T_f/T_0$ where T_f must be interpreted as a magnetic temperature. It is possible to remove the remnant field by heating the solenoid above its superconducting transition temperature. However, this is very inconvenient largely because of the large liquid helium loss involved. A method which avoids actually removing the field from the solenoid is lifting the magnet above the salt pill. Besides technical difficulty this method involves a possible vibrational heat leak. The remnant field can be reduced by "sweeping the field". The current in the magnet is reversed a few times with successively decreasing amplitude. Excessive sweeping must be avoided to prevent eddy current and hysteresis heating of the demagnetization assembly. By manually reversing the current by about 8 amperes the field as measured external to the magnet by a search coil was reduced by a factor of as much as thirty.

Magnetic shielding was used to attempt to reduce the remnant field at the site of the pill. Mu metal shields the remnant field yet reduces the magnetizing field by only a kilo-oersted. The shield was a cylinder of "Netic" mu metal supplied by Perfection Mica Company, Magnetic Shielding

Division (Chicago). The cylinder was about 1/16 in. thick, by 2 in. diameter, by 9 in. length. It was wrapped from annealed foil, each layer being magnetically separated by aluminum foil. It was found that for final temperatures greater than .03 K the remnant field had no measurable effect on the final temperature (using chrome potassium alum).

iii) NMR Field Measurement of Demagnetization Solenoid The demagnetization solenoid was calibrated (field produced by a given current) by observing the nuclear magnetic resonance of aluminum in powder form. Aluminum has a large NMR signal. It was chosen because the resonance frequency of aluminum was in the frequency range of the available marginal oscillator for the field used.

The powder was mixed with oil and placed in a glass tube which was positioned in the centre of the solenoid. Around this specimen tube was wound a coil the inductance of which was determined by trial to give oscillation at about 22 M Hz which corresponds to a field of 20 Kgauss (11.10 M Hz/10.00 KG). The marginal oscillator was modulated at audio frequencies by a transducer or 'wobbulator'. The applied field was swept at 40 gauss per minute. The linewidth of aluminum is 8 gauss so that the signal took about 12 seconds to sweep through. The NMR signal was monitored by a lock-in amplifier and recorded on a strip-chart recorder. The results are given in Table 2.1.

2.3 The Polarizing Solenoid

The polarizing solenoid was wound from superconducting niobium-25% zirconium wire. It was designed to give an approximately uniform saturating field over the specimen yet to give negligible field at the demagnetization salt. The coil was wound with three separated sections on a brass

TABLE 2.1

NMR FIELD CALIBRATION

Run	Resonant Frequency (MHz)	Current in Magnet (amp.)	Field (11.1 MHz/10KG)	Field/Current (KG/amp.)
1	23.36	26.2	21.0	.802
	Sweeping field up			
2	23.14	26.2	20.8	.795
	Sweeping field down			
3	19.38	22.0	17.45	.794
	Sweeping field down			

former. The source was situated between the lower two sections which were wound in the same sense. The third section was wound in the opposite sense to compensate the field produced by the lower sections at the demagnetization salt. The field at the source was estimated to be a half kilogauss per ampere current; the field at the salt about 2% of the field at the source. An experiment which can be used to check the effectiveness of the solenoid is described in the next section.

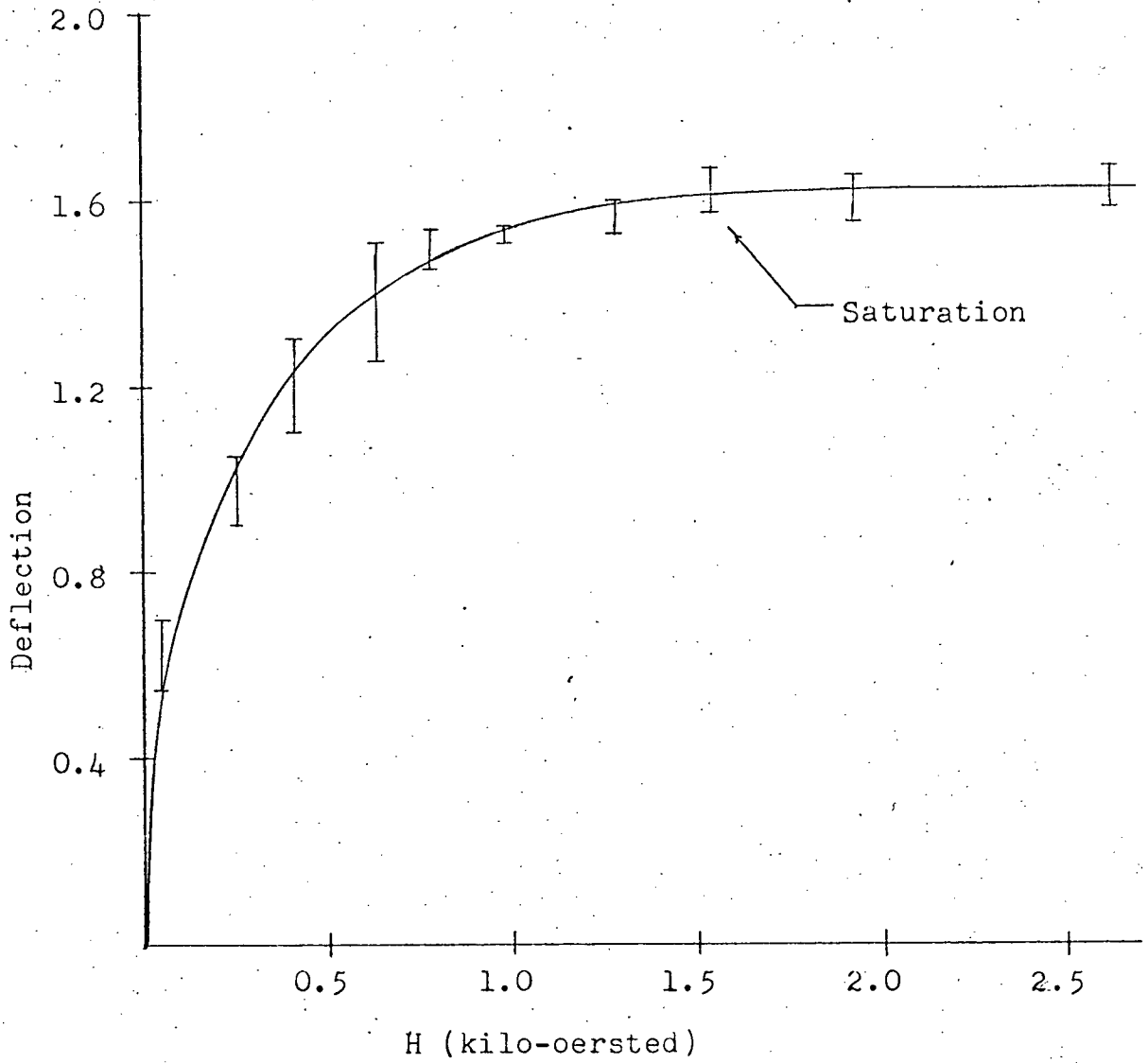
The superconducting leads of the solenoid were spot welded to platinum wires which were soft soldered to copper leads. The current was supplied by a 12-volt storage battery through a transistorized current control unit capable of handling up to seven amperes.

2.4 Magnetic Saturation of Specimen

It was necessary to do an experiment to determine the saturation of the iron foil source. A foil identical to the source was placed in a magnetic field in the orientation used in the nuclear orientation apparatus. Fixed in the field on each side of the foil was a coil aligned with its axis parallel to the field. The coils were connected in series adding through a galvanometer. The experiment was performed by snatching the foil out of the field and measuring the current induced in the coils. This was repeated for different values of the field. The deflection of the galvanometer, D , is proportional to the difference in the magnetic induction B for the foil and for air in the applied field H_0 :

$$D \propto B_{\text{Foil}} - B_{\text{air}} \propto M(H)$$

where M is the net magnetization of the foil. At saturation D is constant for changing applied field. The results of the experiment are shown in



Saturation of Iron Foil

FIGURE 2.2

Fig. 2.2. The saturation field was taken as 1.5 kilogauss. This field required a current of about $3\frac{1}{2}$ amperes in the polarizing solenoid.

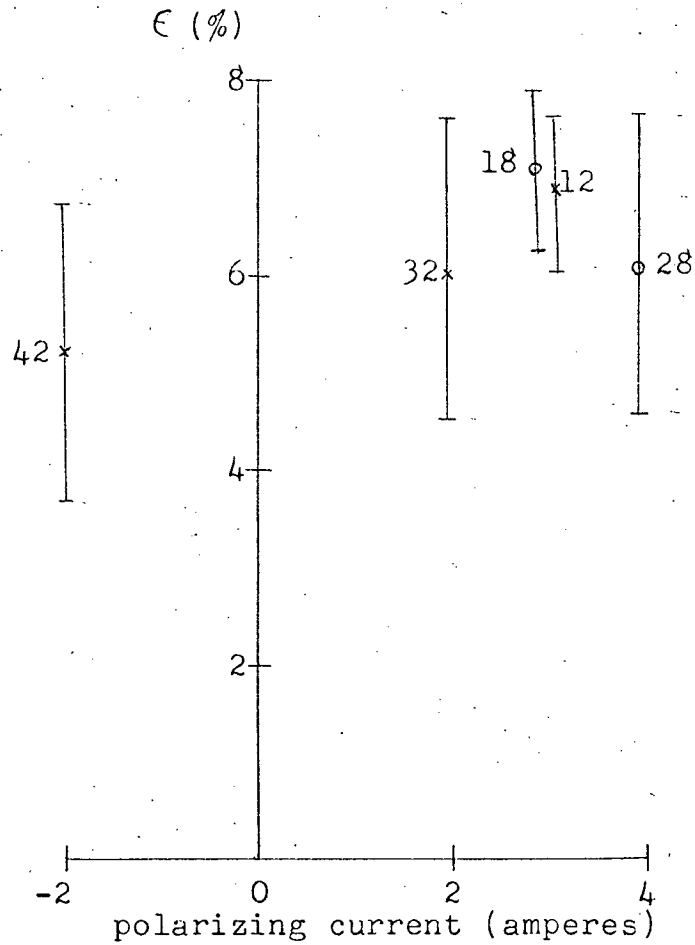
Another experiment was performed to determine saturation during an actual nuclear orientation experiment. The degree of nuclear orientation measured by the anisotropy was measured as a function of the current in the polarizing solenoid. The results are shown in Fig. 2.3. Although no change in anisotropy was observed for currents from two to four amperes no firm conclusions could be reached because of the large errors.

2.5 The Inner Cryostat

i) Description The inner cryostat and demagnetization assembly are shown in Fig. 2.4. The outer can was used as a vacuum jacket to isolate thermally the 1K pumped helium bath. The helium bath in the final arrangement completely surrounded the demagnetization assembly. The inner jacket must be evacuated to isolate thermally the demagnetized salt pills. However, it is also used with helium exchange gas to remove the heat of magnetization. The pumping lines from the outer jacket to the bath jacket are thin-walled stainless steel.

ii) The 1K Helium Bath The helium bath was filled from the 4 K helium reservoir through the pumping line. A needle valve controlled from the top of the apparatus was used to admit the liquid. The bath would be evacuated to a low pressure; then the needle valve was opened allowing the liquid to flow in. Approximately 70 cc. of liquid could be admitted this way. The bath was pumped down by a 5 cubic feet per minute pump (Cenco Hyvac 14). Pressures of about .3 mm. mercury were obtained. This represents a temperature in the bath of ~ 1.2 K.

The heat of magnetization flows into the bath. The maximum heat



Note: The numbers beside the data points indicate the relative time (in minutes) from demagnetization of the reading. See also runs 4 and 5 in Chapter III from which this data is taken (figure 3.7).

Saturation of Specimen (In Situ Experiment)

FIGURE 2.3

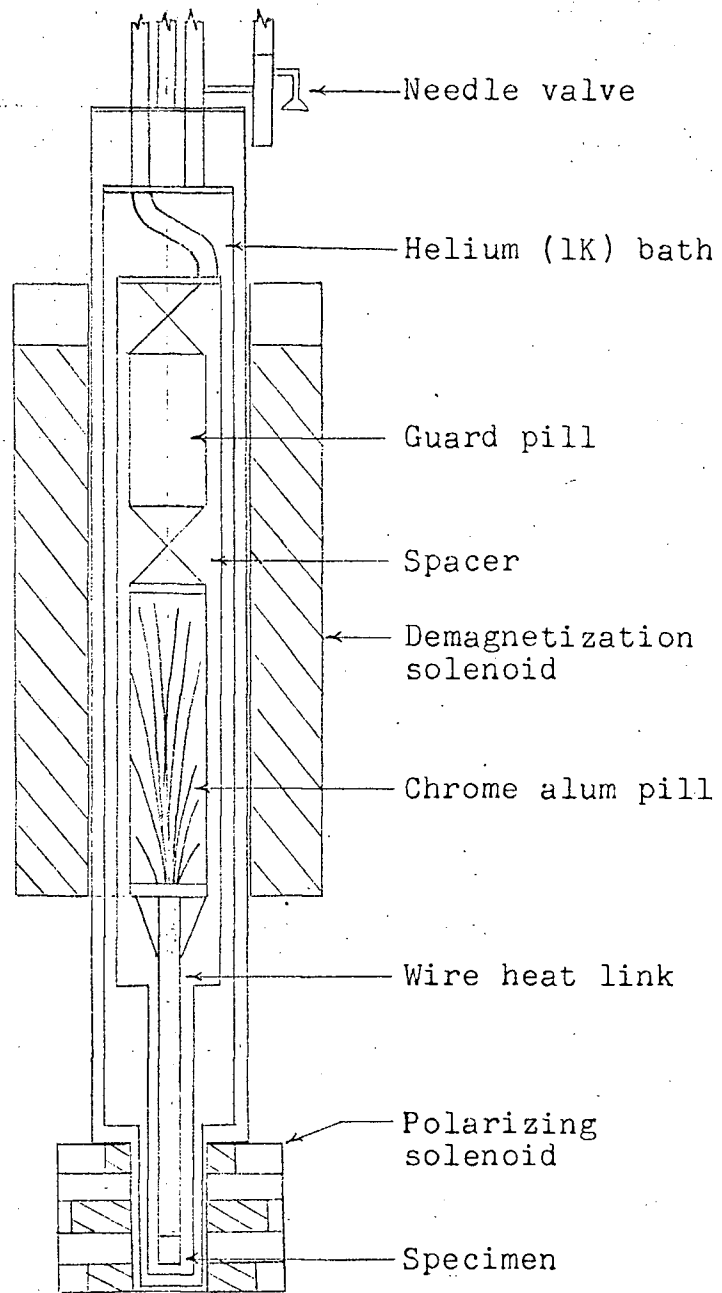
input for isothermal magnetization is given by

$$Q = T\Delta S = TR \ln(2J + 1),$$

where J is the angular momentum of the paramagnetic ions. For 50 grams of chrome potassium alum and 50 grams of manganous ammonium sulphate at 1 K the heat of magnetization is ~ 5 joules which boils off $\sim 1\frac{1}{2}$ cc. of liquid helium. The major loss of helium occurs when it is pumped down. About one half the volume is lost in cooling itself, the jackets and pills. The heat leak to the bath from the outer jacket by gas conductivity is at most 1×10^{-4} W. which is 1/10 cc. of liquid helium per hour. The heat leak down the pumping lines is at most 5×10^{-4} W. or 1/2 cc/hr. Dirt in the pumping line can increase the heat leak by raising the surface area for superfluid creep. The system has been run for as long as six hours and two demagnetizations without running out of liquid helium.

iii) Solder Joins in Inner Cryostat The jackets in the inner cryostat were soldered using low melting point solders to prevent other solder joins from melting during heating. The inner jacket was soldered with a non-eutectic alloy made by melting Wood's metal and radio grade soft solder together to give an over-all melting point about 100°C . The bath jacket and outer jacket were soldered with Wood's metal (melting point = 70°C). Soldering the bath jacket would not melt the inner jacket seal. The solder joins were heated with a natural gas-air torch. Stay-Clean flux, a very corrosive flux, was found useful.

It was necessary to ensure there was no touch between the vacuum jackets. A simple test could be made. The can was soldered in place, then left hanging freely by the solder join. The can was tapped lightly with a metal rod. If the can was not touching it would ring clearly.



Scale:
lin.:1cm.

Inner Cryostat and Demagnetization Assembly

FIGURE 2.4

2.6 The Vacuum Requirements and Low Temperature Vacuum Techniques

There are a number of vacuum requirements in the apparatus. The inner jacket, helium bath (which was discussed in section 2.5), outer jacket, the inner dewar space and the inner dewar interspace all require use of low pressure.

i) The Inner and Outer Jackets The inner and outer jackets require very high vacuum for thermal isolation yet they require also the use of helium exchange gas. The inner jacket should be capable of maintaining a vacuum of the order of 10^{-6} mm. of mercury (measured at room temperature) during a demagnetization without external pumping. The outer jacket should be able to maintain a pressure of 2×10^{-5} mm. of mercury without pumping (with the helium bath pumped down). These requirements were met using a 2 in. metal oil-fractionating diffusion pump (Consolidated Vacuum Corporation, PMC-115) pumping through a glass manifold system into 3/8 in. copper pipe to the cryostat. The diffusion pump requires a rotary fore-pump (Cenco Hyvac 7) of at least 3 cubic feet per second. The outer jacket would be pumped down to 5×10^{-5} mm. of mercury before pumping the helium bath. Then the outer jacket was shut off. Upon pumping the bath the outer jacket pressure would fall to $\sim 2 \times 10^{-5}$ mm. of mercury pressure.

Pumping on the inner jacket was eliminated (pumping rates are very low at low temperatures) by using the following technique. The exchange gas pressure in the inner jacket was set at .01 mm. of mercury before the bath was pumped. Upon pumping the bath the pressure in the inner jacket would fall to less than 2×10^{-4} mm. of mercury. Upon demagnetization the pressure would fall to less than 5×10^{-6} mm. of mercury (through absorption of the exchange gas in the pills).

The pumping manifold contained a cold trap to prevent pump vapours from contaminating the system. The helium exchange gas was supplied by a glass flask connected to the manifold. Inner and outer jacket pressures were measured at the manifold by cold cathode Phillips gauges.

ii) Other Pumping Requirements The helium bath was pumped to .3 mm. of mercury by a 1 in. pumping line. The pressure was measured by mercury and oil manometers at high pressure and by a thermocouple gauge at low pressure (1 to 10^{-3} mm. of mercury range) for accurate measurement. There is a large gas load upon initial pumping of the bath which requires a fairly large pump. A five cubic feet per minute pump was found to be sufficient.

It was required that the liquid helium 4 K reservoir and the inner dewar interspace be flushed with helium gas. Any rotary pump served these vacuum needs. The backing lines of the manometers were pumped by the fore-pump of the diffusion pump.

2.7 The Paramagnetic Salt Assembly

i) Chrome Potassium Alum Pill The chrome potassium alum salt pill (see Fig. 2.4) was made from a slurry of alum and glycerine. The mixture becomes a glass at low temperatures giving good thermal contact to the heat link. The slurry was made by mixing finely ground chrome alum powder with a 50-50 solution of glycerine and alum-saturated water. The consistency was that of a thin jam. The mixture was added as uniformly as possible to the wire or copper fin heat link. The entire assembly was then put in the bakelite pill. A 33 ohm Allan-Bradley resistor had previously been fixed in contact with the alum mixture in the top of the pill. This resistor was used as a thermometer above 1K to measure the

precooling of the pill and as a heater after demagnetization for warming the specimen assembly prior to taking normalization counts. The leads to the resistor were constantan wire (80 ohms per foot) wrapped many times around the supporting tubes above the alum pill.

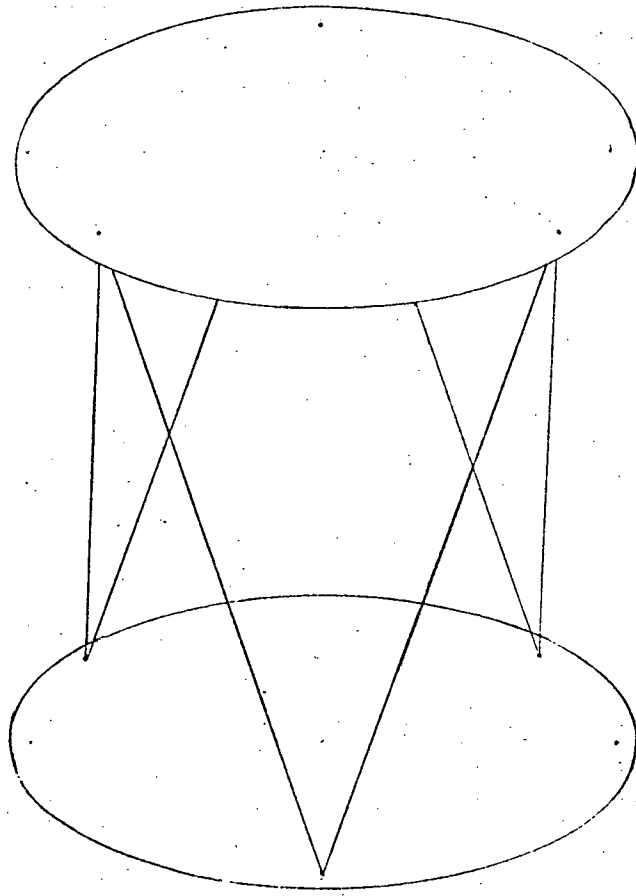
ii) The Guard Pill The manganous ammonium sulphate salt pill served as a guard pill against leaks down the supports to the chrome alum. Manganous ammonium sulphate demagnetizes to about a tenth of a degree Kelvin in a field of a few kilogauss. The pill was made from ground manganous ammonium sulphate powder. It was contained in a light brass can. Twelve copper fins were soldered in the can to give a surface area of 100 cm^2 .

iii) The Spacers The thermal isolation between the two salt pills and between the guard pill and the bath was provided for by spacers. Each spacer was made from 6 1 mm. outer diameter by .1 mm. wall german silver tubes each about $2\frac{1}{2}$ cm. long soft soldered in brass end pieces. The arrangement of the tubes provided high rigidity and low sectional area. The arrangement is shown in Fig. 2.5. The heat leak to the chrome alum down the spacer is expected to be less than 20 erg/min.

2.8 The Heat Link and the Specimen Temperature

The heat link between the source and demagnetization pill was made from about 5000 B and S gauge 44 copper wires. The wires were enamel-coated to prevent eddy current heating during the demagnetization and to prevent corrosion by the chrome alum. The surface area in contact with the alum was about 900 cm^2 . The ends of the wires were cleaned with stripvar enamel remover and soft soldered into a standard 3/8 in. copper coupling. The coupling was hard soldered to a 3/8 in. copper rod to

Brass
end-pieces



German
silver tubes

The Spacers

FIGURE-2.5

which the iron specimen foil was soft soldered. The iron foil was first "tinned" using Stay Clean solder flux and then soldered to the copper using the same flux. A copper foil heat link with a contact area of 800 cm² was also used. The copper wires or foil were fastened to the bakelite salt pill container and held straight and rigid by a low temperature epoxy resin.

The heat removed from the copper heat link and all other materials must be absorbed by the alum. The lattice heat capacities are all negligible below 1°K compared to the electronic specific heat of the copper. Cooling the copper removes heat $dQ = CdT$, where C is the electronic specific heat. This heat flows to the alum giving an increase in entropy as given by $dQ = TdS$. Integrating from 1K to 1/100 K using $C = .888 \times 10^{-4} RT$ gives:

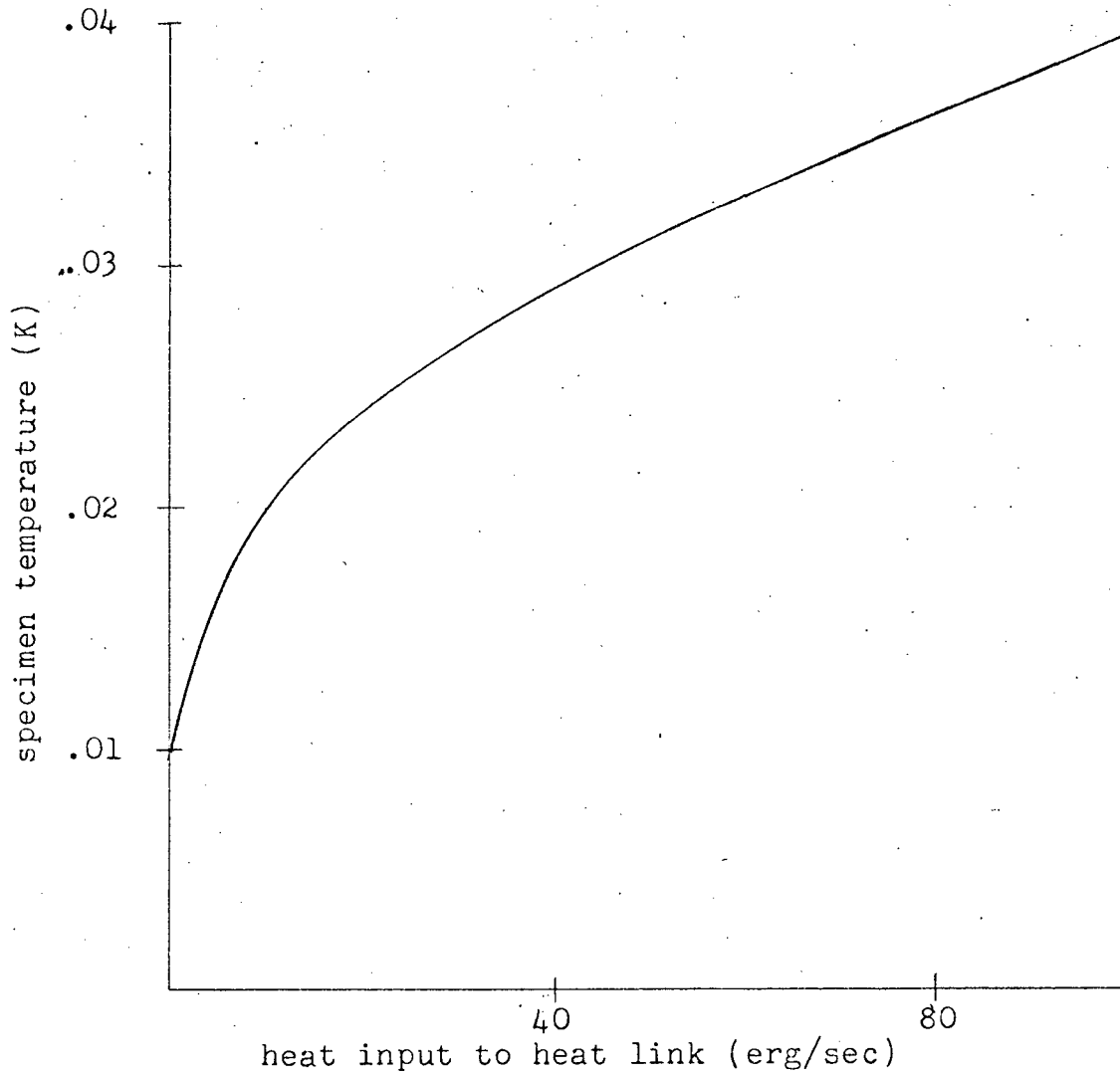
$$S = 1 \times 10^{-4} \text{ j (K)}^{-1}$$

This figure is about .005% of the total entropy removed by the magnetization and is negligible.

Using the theoretical results given in the introduction, a curve giving the final temperature of the source against the heat leak into the wires has been plotted in Fig. 2.6. It has been assumed all wires or fins make full contact with the alum.

A specimen source radiation strength of 17 microcurie emitting one Mev. of energy absorbed in the source (beta radiation) gives a heat leak of about one erg per sec. In these experiments source heating was kept below one tenth of an erg per sec.

Heating of the source by gas conductivity from the walls of the inner jacket can be calculated to an order of magnitude. An expression



The Specimen Temperature

FIGURE 2.6

for the heat transfer is¹⁶

$$\dot{Q} = \text{const} \cdot a_o \cdot p_{\text{mm}} \cdot (T_1 - T_2) \text{ W cm}^{-2}$$

for two parallel surfaces at temperatures T_1 and T_2 . Here the constant is .028 for helium and a_o , the accommodation coefficient, is not greater than 0.5 for normal laboratory situations. The gas pressure, p_{mm} , is measured in mm. of mercury at room temperature. For a pressure 1×10^{-6} mm. of mercury and an exposed copper surface area of 50 cm^2 the heat leak is

$$\dot{Q} \approx 8 \text{ erg sec}^{-1}.$$

This gives a predicted lowest temperature of .020 K at the specimen.

Unfortunately, the actual partial pressure of helium gas is not readily known because of outgassing of volatile vapours near the pressure gauge. These vapours are not expected to reach the pill or wire assembly.

Eddy currents induced by vibration of the copper in the magnetic field could be a significant heat leak if the current path is long.

A heat conducting sleeve over the heat link and alum pill, but not in contact with them, thermally anchored to the guard pill would reduce the gas conductivity heat leak and the heat leak caused by adsorption of helium gas on the wires and alum pill. However, in practice such a shield gives only a marginal improvement.

2.9 Vibrations

Vibrations can present a significant heat leak in the demagnetized system. Indeed, even at 1K the vibrations can heat the pill at low exchange gas pressure. The major sources of vibrations of the apparatus are expected to arise from the building itself through the floor or any other mechanical contact, from pumps including diffusion pumps, from bubbling of the liquid

refrigerants and from handling the apparatus. It is extremely important that resonant conditions be avoided. Hence everything in or on the apparatus must be firmly attached and the entire assembly made as rigid as possible.

The apparatus was built on an aluminum Dexion frame reinforced as much as possible. The entire assembly was placed on steel spring vibration isolators. Cement blocks were placed in the bottom for damping. The pumping lines inside the cryostat were reinforced for rigidity. The demagnetization assembly was made as rigid as possible. The bath pump was connected to the apparatus by flexible rubber tubing. At the pump itself, the pumping line was firmly anchored to the building.

During the demagnetization personal contact with the apparatus was avoided. Both the diffusion pump and the mechanical fore-pump were stopped.

In spite of these precautions some vibrations were still present in the apparatus and could be detected by an accelerometer. The extent of the vibration heat leak has not been determined. However, only after all these steps had been taken could runs be done with consistent success.

2.10 Experimental Procedure

The demagnetization solenoid was charged to 44 kilogauss (55 amperes) with the helium bath initially at 1.2 K. Occasionally, to save time or to calibrate the pill resistor (in the magnetic field) the magnetization was done at 4.2K, the bath being pumped after or during magnetization. The outer jacket would be pumped to about 5×10^{-5} torr. The initial exchange gas pressure in the inner jacket was set at .01 torr at 4.2K as described in section 2.6 i). At 1.2K the inner jacket pressure would fall to 2×10^{-4} torr or less. During magnetization the inner jacket pressure would

rise to about 5×10^{-3} torr. The bath pressure would rise slightly (depending on the pump speed). After the magnetization the inner jacket pressure and the resistance of the carbon resistor in the pill were monitored. When these measurements indicated cooling had completed (about 25 minutes) the demagnetization was begun. The demagnetization should be done sufficiently slowly to keep eddy currents induced as small as possible yet sufficiently fast to quickly lower the inner jacket pressure and keep vibrational eddy current heating small. Initially, the field was reduced at a rate of 6 kilogauss per minute. The inner jacket pressure would quickly fall. When the field had reduced to 4 to 5 kilogauss the demagnetization was stopped until the exchange gas pressure stopped falling (1-2 minutes). It is desirable to remove the exchange gas at a high temperature if possible ($dQ = T dS$). The demagnetization was recommenced at a rate of 3 kilogauss per minute until no current was flowing. The polarizing coil was charged to 3 amperes. The current in the demagnetization solenoid was reversed to sweep out the remnant field. When the remnant field as measured by search coil outside the cryostat was reduced as low as possible the counters were carefully put in place and gamma ray counting was started. By this time the inner jacket pressure gauge reading would be $2 - 5 \times 10^{-6}$ torr. When sufficient cold counts had been taken the pill would be warmed by electrically heating the carbon resistor in it. For additional runs the magnet was recharged and the procedure repeated. A typical low temperature run as taken from the log book is given in Table 2.2.

TABLE 2.2

TYPICAL LOW TEMPERATURE RUN

This table gives the procedure as taken from the laboratory notebook for run 7 in Table 3.1.

<u>Time</u>	
	System precooling overnight with liquid nitrogen. Helium exchange gas in outer, inner and bath jackets.
14:15	Liquid helium transfer is in progress. Liquid helium is in bottom of dewar. Transfer pressure head is 2 cm. mercury.
:35	Transfer completed. About 12 litres of liquid helium were used. Resistance of carbon resistor in chrome alum pill (R_p) is 1.23K ohm. Bath filled.
:50	Beginning pumping of outer jacket.
15:24	Outer jacket shut off. Outer jacket pressure is $5\frac{1}{2} \times 10^{-5}$ torr. This is sufficiently low to pump bath. Inner jacket pressure is .005 torr (at 4.2K). $R_p = 1.23K$ ohm (no magnetic field).
:35	Begin magnetization (at 4.2K).
:41	Magnet is in persistent mode at 55 amp. Bath was refilled to replenish any liquid lost in magnetization.
:43	$R_p = 1.38K$ ohm Will begin pumping bath.
16:27	Outer jacket pressure is 3×10^{-5} torr.
:30	$R_p = 15.1K$ ohm Inner jacket pressure is 1.8×10^{-4} torr.
:40	$R_p = 15.2K$ ohm. Assume pill has cooled to bath temperature.

:40 Inner jacket pressure is 7×10^{-5} torr.
(cont'd) Bath pressure is approximately .3 torr. This pressure
means the bath temperature is 1.1K.
Diffusion and backing pumps turned off in preparation for
demagnetization.

17:00 Begin demagnetization.

:05 Demagnetization completed.

:07 Polarizing solenoid charged to 3 amp.
Commencing counting.
Inner jacket pressure is $1\frac{1}{2} \times 10^{-5}$ torr.

:10 Measure remnant field with search coil: deflection of +3 cm.

:22 Swept field by reversing current in demagnetization solenoid
to -8 amp.
Measure remnant field: deflection of -1/3 cm.

:55 Pill warmed by electrically heating resistor in chrome alum
pill.
Commencing normalization counts.
Inner jacket pressure is 1.8×10^{-4} torr.

18:26 End of first run. Anisotropy achieved 8%.

:33 Begin next magnetization, etc.

CHAPTER III

NUCLEAR ORIENTATION OF ^{60}Co IN IRON

The nuclear physics aspects of the experiment are considered in this chapter. The choice of ^{60}Co as a thermometer is discussed. The preparation of the source and the electronic set-up is also discussed. Finally the actual low temperature experimental data is presented and the analysis of the results.

3.1 The Temperature Dependence of the Anisotropy of ^{60}Co

^{60}Co was chosen for three reasons: i) Its nuclear and hyperfine parameters are well known; ii) It has a large anisotropy at a hundredth of a degree Kelvin; and iii) It is readily available and dissolves easily in iron.

The decay scheme for ^{60}Co is shown in Fig. 3.1. The magnetic moment of ^{60}Co is equal to 3.754 (± 8) nuclear magnetons¹⁶. The hyperfine field of dilute cobalt in iron foil is 290 kilogauss¹⁷. The equations for the intensity of radiation given in Chapter I reduce to

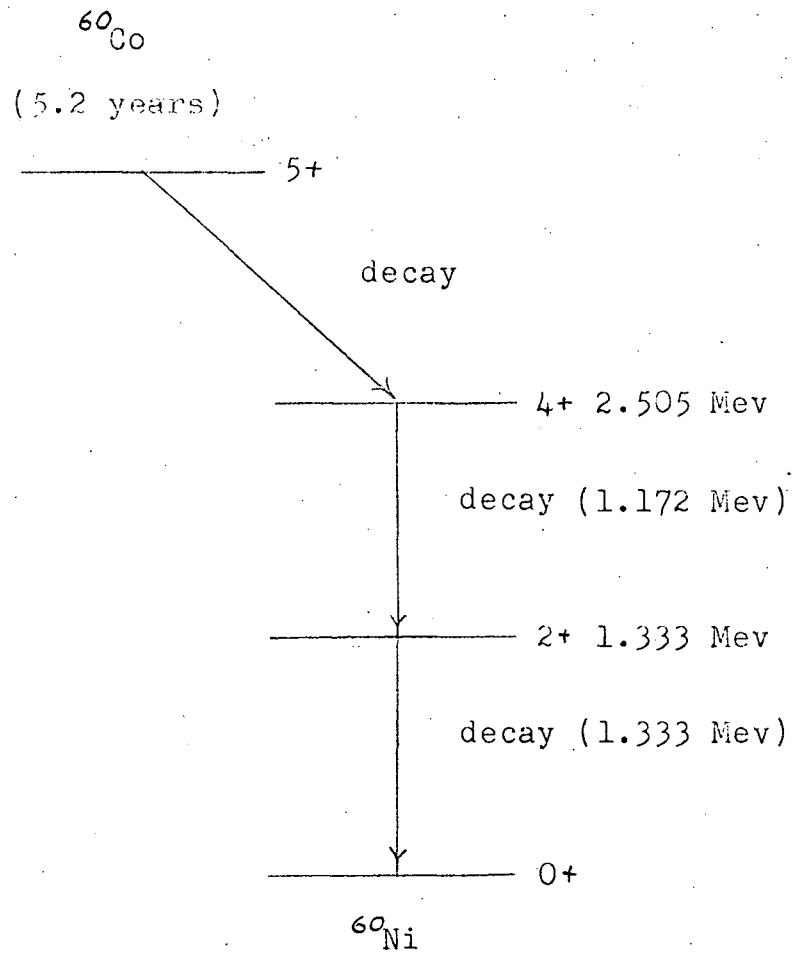
$$W(0) = 1 + U_2 F_2 B_2 + U_4 F_4 B_4$$

$$W(\pi/2) = 1 - \frac{1}{2} U_2 F_2 B_2 + \frac{3}{8} U_4 F_4 B_4$$

The U coefficients reduce to (see reference 4, p. 1206)

$$U_i = (-1)^{(I_0 + I_1 - L_1)} (2I_0 + 1)(2I_1 + 1)^{\frac{1}{2}} W_{(I_1 I_1 I_0 I_0, iL)}$$

where I_0 , I_1 are the angular momenta for the initial and final states of the unobserved transition and L_1 is the angular momentum carried away in



The Decay Scheme of ^{60}Co

FIGURE 3.1

this transition. W is the Racah coefficient. The F coefficients are given in reference 4, p. 1197. Using these results the parameters are

$$U_2F_2 = -0.421; \quad U_4F_4 = -0.243$$

for both gamma decays. The B coefficients are given in reference 3. The final temperature dependence of $W(0)$, $W(90^\circ)$ and ϵ is given in Fig. 3.2.

3.2 The Preparation of the Source

The ^{60}Co source was prepared from a cobalt chloride solution containing ^{60}Co with virtually no ^{59}Co carrier present. The cobalt is less electropositive than iron. Hence, when drops of cobalt solution are placed on the iron foil, the foil is spontaneously plated by cobalt. The foil was annealed at 950°C for 24 hours in a dry hydrogen atmosphere. The activity of the source was determined by counting against a known strength source. The source was then etched and its strength remeasured. As there was no decrease in activity it was concluded that the cobalt had diffused well into the iron. The final activity was about $2\frac{1}{2}$ microcuries.

3.3 The Detectors and Electronic Circuitry

The gamma radiations were normally detected by sodium iodide crystal scintillation detectors. The crystals were 2" x 2" mounted on a photomultiplier. The photomultipliers were very sensitive to magnetic fields which meant they had to be shielded from the polarizing field. Sufficient shielding was provided by a soft iron pipe 3" diameter by 1/4" wall thickness (with a very low impurity gamma radiation activity) which was slipped over mu metal which was wrapped around the detector and spaced with copper foil. The effect of the polarizing coil on the counting rate was smaller than the statistical counting error provided the detectors were

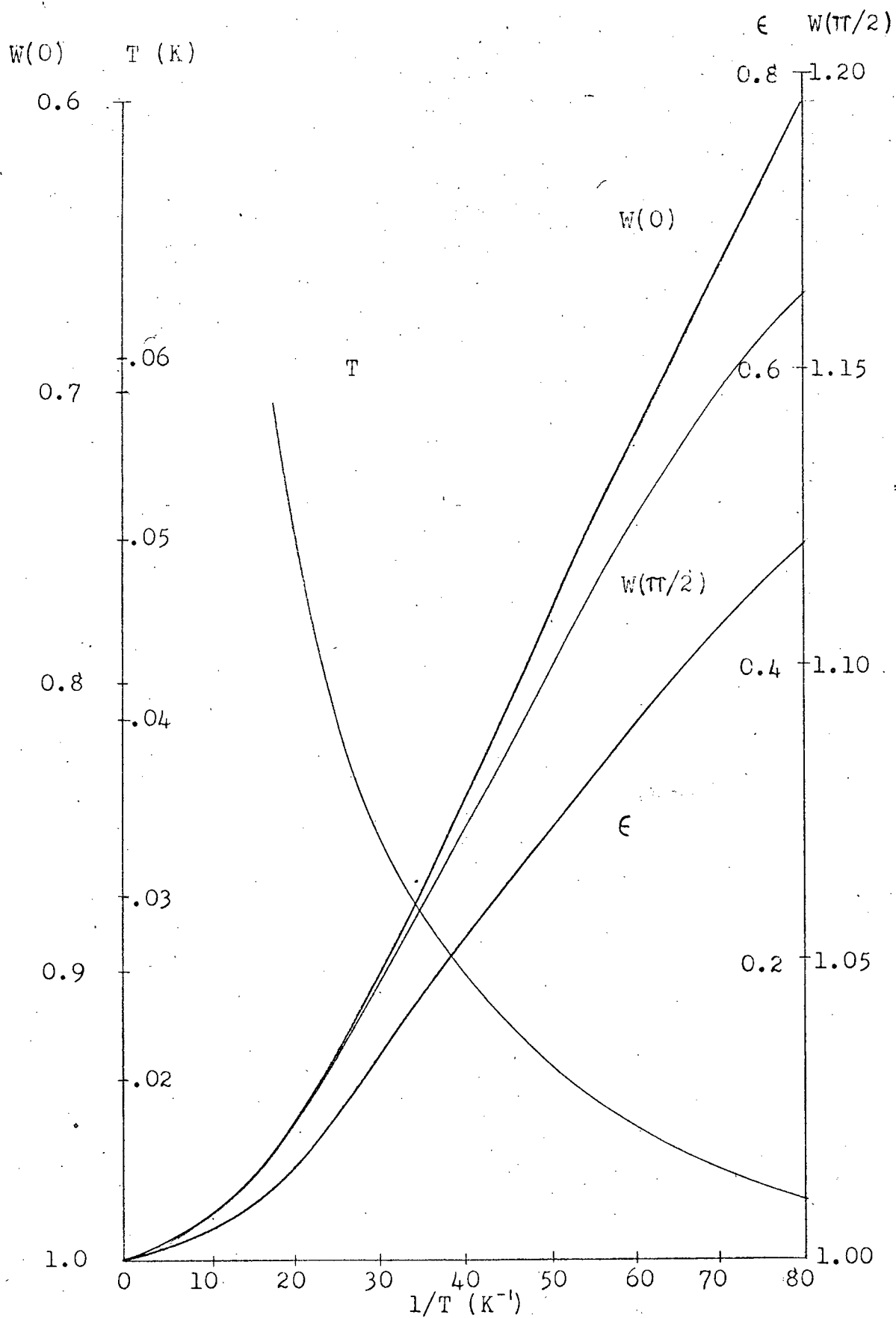


FIGURE 3.2 The ^{60}Co Thermometer

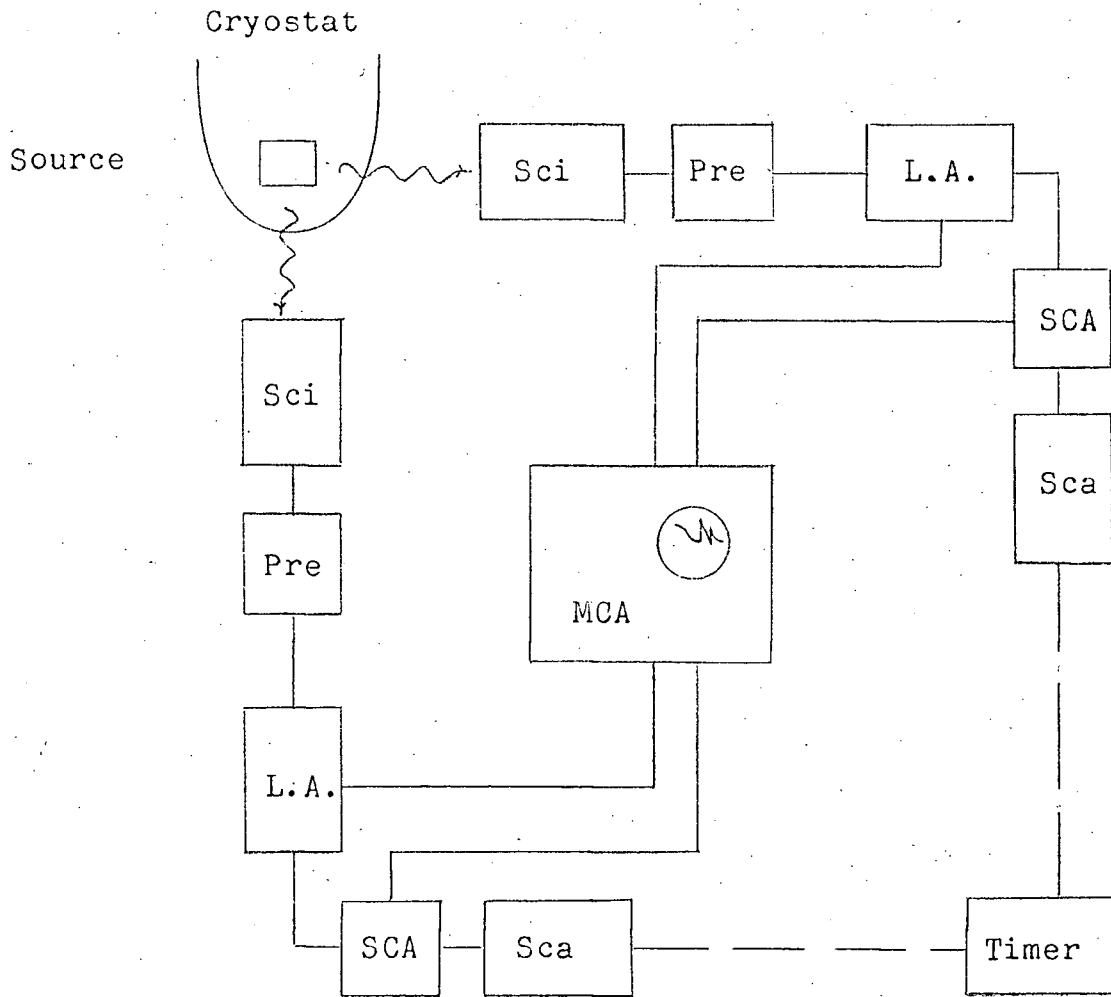
not too close to the outer dewar. In any event, the counts were normalized with the same fields present if possible. Any change in the gain of the detectors could be detected on the multi-channel analyser discussed below.

The electronics used are shown schematically in Fig. 3.3. The resolution of the system was sufficient to separate the ^{60}Co gamma ray photopeaks almost to the baseline. The multichannel analyser was used (in the pulse height analysis mode) to set the single channel analyser windows and to determine any change in gain of the system. It was also used to obtain spectra so that the radiation background could be stripped off the photopeaks. In addition, the analyser has a multi-scaling mode which can be used to run up the counts from each detector switching channels automatically after a given counting time. The counts can then be punched out on tape. In this way the actual counting time will be increased because the delay of recording the counts is eliminated. Also, errors in recording are eliminated. The warm-up of the source can be readily seen on the oscilloscope output at any time. The punched tape output can readily be used for computer analysis of the data.

In one run a Ge(Li) solid state detector was used in the equatorial plane. It gave very good resolution of the two ^{60}Co gamma photopeaks well past the baseline. This detector was not affected by the magnetic fields present.

3.4 The Experiments: Data and Results

i) The Raw Data It was usual to take a few sets of counts shortly before the demagnetization or after the demagnetization but before the polarizing solenoid was charged in order to obtain some idea of the normalization counts. They were also useful for determining any change



Sci Sodium iodide scintillation detector
 Pre Preamplifier
 L.A. Linear amplifier
 SCA Single channel analyzer
 Sca Scaler
 MCA Multi-channel analyzer and routing

The Gamma Radiation Detection Apparatus (Schematic)

FIGURE 3.3

in the gain of the detectors in the field of the polarizing solenoid. When the demagnetization was completed (including sweeping the field) the experimental counting was commenced. The scalers were operated either by hand or by a master timer. Counts were usually taken for 100 to 200 sec. periods. The scaler digital readings were recorded by hand. After the sample was warmed the normalization counts were taken. Care was taken to ensure that no change in the magnetic fields on the counters occurred during the run (unless such changes were part of an experiment). The warm counts were taken for the same period as the cold counts to get an idea of the random variations. A few long warm counts would then be taken to reduce the statistical error. The raw counts for a number of runs are shown in Table 3.1.

The window settings of the single channel analysers were usually set to show the total counts in both the 1.17 and 1.33 Mev photopeaks of the ^{60}Co since both gamma rays show the same anisotropy.

ii) Corrections to the Raw Data The isotropic background of the laboratory must be subtracted from the raw counts taken during the experiments. For the runs reported in this work the isotropic background was less than 1% of the total counts. In the normalized counts the correction is less than 1/5% and has been neglected. The anisotropic background in the photopeaks from scattered radiation must also be subtracted. In the present experiment no higher energy radiations were present to give background to the ^{60}Co photopeaks. Hence, this correction is negligible.

The half-life of ^{60}Co is 5.2 years. Hence, no correction need be applied for the decay of the source during the run.

There is a correction for the "smearing out" of the anisotropy due

to the solid angle subtended by the counters. The spatial distributions of radiation was shown in Chapter I to be of the form:

$$W(\theta) = \sum_i A_i P_i(\cos \theta)$$

This function must be modified to include the solid angle subtended by the counter from the source as follows

$$W'(\theta) = \frac{\int_{\Omega} W(\theta) d\Omega}{\int_{\Omega} d\Omega}$$

where Ω is the solid angle of the counter. It has been shown that for cylindrical counters the form of the distribution function is unchanged but that each term becomes multiplied by an attenuation factor independent of the angle of observation¹⁸. Hence,

$$W'(\theta) = \sum_i A_i P_i(\cos \theta) k_i(\alpha)$$

where α is the linear half-angle subtended by the cylindrical counter.

The attenuation coefficients k_i can be calculated directly by integrating the Legendre polynomials giving¹⁹:

$$k_2 = \frac{1}{2} \cos \alpha (1 + \cos \alpha)$$

$$k_4 = \frac{1}{8} \cos \alpha (1 + \cos \alpha) (7 \cos^2 \alpha - 3).$$

In the experimental runs reported in this thesis the counters used 2" x 2" crystal detectors, except one run which used a Ge(Li) solid state detector in the equatorial plane. The axial counter was 6" from the source and the equatorial counter was 5" from the source. Using the approximation of 2" cylindrical counters and a point source the attenuation coefficients are

$$k_2 = .97 \text{ and } k_4 = .90$$

for both counters. For anisotropy ϵ of 10% or less the correction to ϵ is less than +1/3%. This correction has been neglected. The geometry of the Ge(Li) detector was not known; however, the attenuation was small and the correction factor has been ignored.

iii) The Results The analysis of several runs are given in Table 3.1 and Figs. 3.4 to 3.9. In run 2 (Fig. 3.5) the effect of reversing the polarizing field is shown. Also shown is the length of run before warming occurs. At 30 minutes after the demagnetization the anisotropy was still observable. Run 3 in Fig. 3.6 gives an uninterrupted run showing the warming of the pill beginning about 20 minutes after demagnetization. Runs 4 and 5 (Fig. 3.7) show the effect of different polarizing fields. In these two runs the demagnetization assembly and conditions were the same. In this case warming occurs too quickly to draw significant conclusions about the effect of the polarizing solenoid. The effect of the remnant field was studied in run 6 (Fig. 3.8). The pill was unshielded. The remnant field was gradually swept out. No significant change in anisotropy was noticed although the remnant field was reduced by a factor of ten (as measured by a search coil external to the cryostat). In run 7 (Fig. 3.9) only 8 g. of chrome alum was used in the pill. However, a significantly long run was performed with a relatively high anisotropy (7.4%). This would indicate that the amount of alum used normally, 30 - 60 g., was sufficient for cold times of about a half hour.

During the course of the runs, several chrome alum mixtures were used; two wire heat links and one fin heat link were used and two specimen sources were tried. No significant differences in results were noticed in any case.

TABLE 3.1

Time	Counting Period	Raw* Counts Axial	Raw* Equa- torial	Normalized (0) Axial	Normalized (90°) Equa- torial	€ %	T (K)
All errors quoted represent one standard deviation in the counting statistics							
Run 1	(24th July, 1968)	Basic counting period 6 minutes					
9:03	Demagnetized						
	Polarizing field = 0 (Pseudo warm count)						
	2 min.*	19041	27573				
	Polarizing field = 4A						
:08	6 min.	17739	29158	.937±1%	1.048±1%	(10½±1)%	.038±.001
:15	"	17667	28743	.932	1.037	(10.±1)%	.038
:21	"	17484	28878	.923	1.039	(11.±1)%	.036
:29	"	17736	28762	.937	1.032	(9.±1)%	.043
Normalization Counts							
	12 min.*	19071	27783	} (18940)	(27794)		
	6 min.	18715	27710				
	6 min.	18904	27921				
Run 2	(7th October, 1968)	Basic counting period 300 seconds					
	Polarizing field = 0A.						
8:55	(3x) 100 sec.	13803	74052				
	Polarizing field = 4A.						
:57	3 x 100 sec.	13417	73766	.973±1½%	1.020±½%	(4.7±1½)%	.059±.008
9:03	"	13363	73516	.969	1.018	(5 ±1½)%	.056
	Polarizing field reversed						
:27	"	13469	73298	.976	1.010	(3.4±1½)%	.07
	Original polarizing field						
:45	3 x 100	13448	72756	.984	1.005	(2±1½)%	.1 ±.06
	Normalization						
	3 x 100	13788	72309				

*The raw counts not in basic counting period are multiplied by the factor necessary to make them comparable to the basic counting period.

Time	Counting Period	Raw* Counts Axial	Raw* Counts Equatorial	Normalized (0) Axial	Normalized (90°) Equatorial	ϵ %	T (K)
Run 3	(1st November, 1968)	Basic counting period		300 seconds			
12:34	Demagnetization.	Polarizing current = 0A.					
	(3x) 100 sec.	12441	42813				
	Polarizing field = 4A.						
12:37	3 x 100 sec.	11992	43010	.976	.996	(2.±1½)%	.1 ±.06
:46	"	11910	43746	.959	1.010	(5.±1½)%	.056±.006
:52	"	11942	43517	.962	1.005	(3.3±1½)%	.07
:58	"	12156	43194	.979	.999	(2.±1½)%	.1 ±.06
1:02	"	12363	43322	.995	1.002	(.7±1½)%	.049±.006
1:06	"	12499	43767	1.005	1.012	(.7±1½)%	.049
	Normalization						
	1100 sec.*	12410	43220				
Run 4	(7th June, 1969)	Basic counting period		3 minutes			
5:35	Demagnetization, Polarization Current & 3 Amps.						
	3 min.	4513	16022	.955	1.021	(6.5±2)%	.05 ±.006
	"	4473	16240	.946	1.035	(7.6±1½)%	.046±.006
	"	4476	15895	.947	1.013		
	"	4558	15890	.964	1.013	(7.2±1½)%	.049±.006
	"	4394	16097	.931	1.028		
	"	4562	15987	.966	1.020	(6.6±1½)%	.049±.006
	"	4512	16229	.955	1.037		
	Polarizing field + 4 Amp.						
6:02	4 min.*	4500	15950	.952	1.018	(6.0±1½)%	.052±.006
	3 min.	4557	15880	.965	1.011		
	"	4602	15637	.974	.998	(2.5±1½)%	.09 ±.06
	"	4743	15806	.983	1.009		
	"	4633	16020	.980	1.021	(3.3±1½)%	.07
	"	4564	15731	.976	1.002		
	"	4755	15635	1.005	.998		
	"	4672	15964	.988	1.018	(3.0±2)%	.08

Time	Counting Period	Raw* Counts Axial	Raw* Counts Equatorial	Normalized (0) Axial	Normalized (90°) Equatorial	ε %	T (K)
------	-----------------	-------------------	------------------------	----------------------	-----------------------------	-----	-------

Polarizing field + 3 Amps.

:32	3 min.	4626	15766	.986	1.006	(2.0±2)%	.1
	9 min.*	4722	15883	1.000	1.011	(1.1±1½)%	.14
:48	9 min.*	4611	15689	.974	1.000	(2.6±1½)%	.09 ±.06

Normalization

18 min.*	4745	15662	} (4726) (15681)
18 min.*	4706	15700	

Run 5 (7th June, 1969) Basic counting period 3 minutes

Demagnetized, polarizing current + 3 Amps.

11:23	3 min.	4602	18035				
	"	4559	18010		17924		
	"	4488	17855	.954	1.032	(7.6±.1½)%	.046±.006
	"	4527	17796				
:35	"	4561	18159				
	"	4774	17757	.971	1.035	(6.2±.1½)%	.051±.006
	"	4581	18115				
	"	4589	17886				

Polarizing current + 2 Amps.

:48	3 min.	4586	17888				
	"	4600	17811	.967	1.018	(5.0±1½)%	.056±.006
	"	4599	17521				
:12	"	4723	17383	.987	1.003	(1.6±1½)%	.12
	"	4680	17458				

Normalization

18 min.*	4800	17218	} (4765) (17364)
18 min.*	4730	17510	

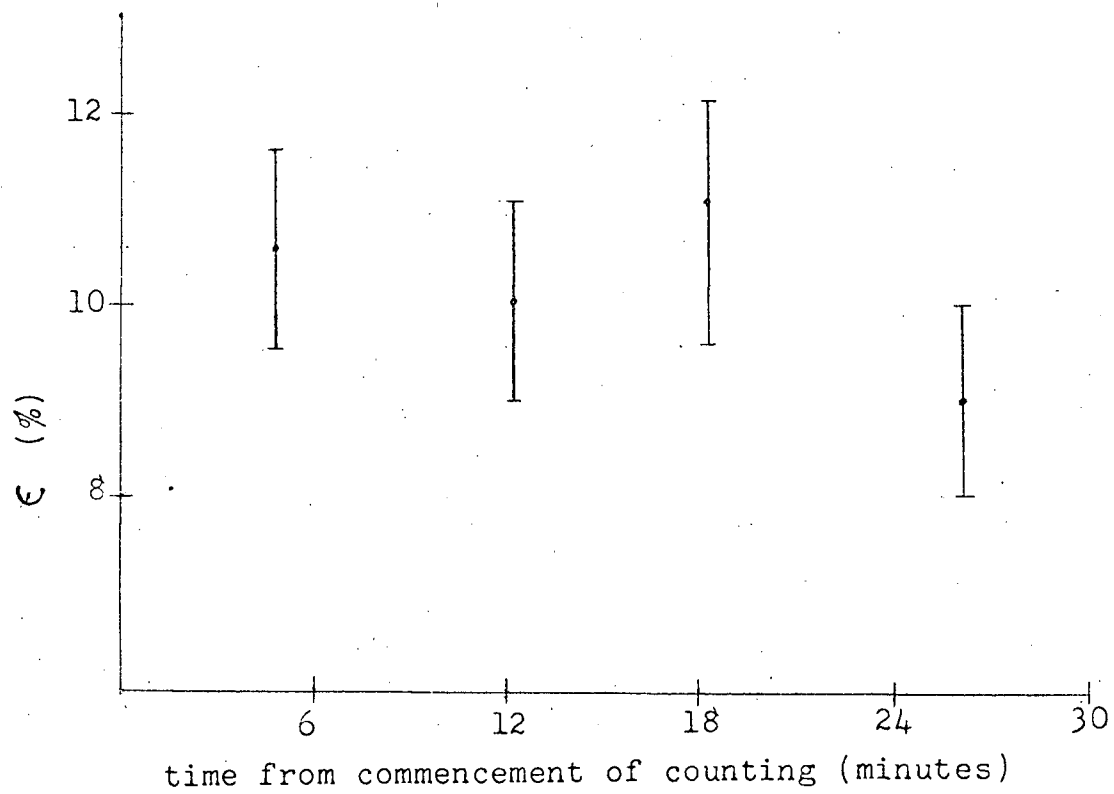
Run 6 (2nd run) (12th June, 1969) Basic counting period 3 minutes

16:30 System demagnetized

Search coil reading of residual field = 0.8 cm. deflection

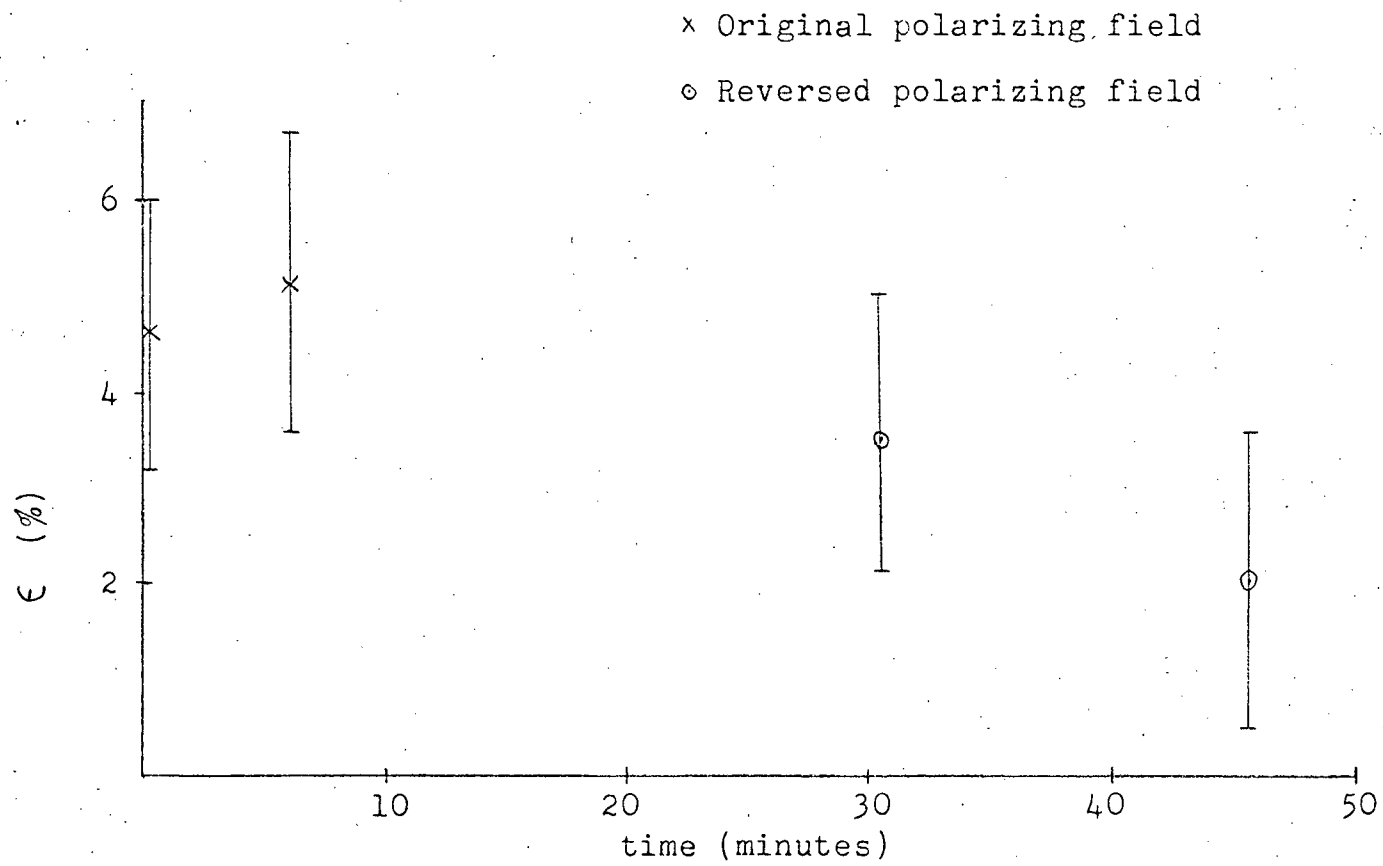
Time	Counting Period	Raw* Counts Axial	Raw* Counts Equatorial	Normalized (0) Axial	Normalized (90°) Equatorial	€ %	T (K)
	3 min.	4858	19884				
:33	"	4788	19851	.936	1.011	(7.4±1½)%	.047±.006
	"	4907	19825				
Sweep field. Search coil = +.3 cm. deflection							
:42	3 min.	4840	20097				
	"	4867	20269	.934	1.028	(9.1±1½)%	.042±.005 ^{+.002}
	"	4812	20199				
Sweep field. Search coil .1 cm. deflection							
:54	3 min.	4976	20275				
	3 min.	4913	19996	.945	1.021	(7.4±1½)%	.047±.006
	"	4803	19900				
	"	4871	20124				
	"	4672	19779	.938	1.016	(7.7±1½)%	.046
	"	5031	19979				
Normalization							
	5 x 3 min.*	5181	19645				
Run 7 (1st run, 8th August, 1969) Basic counting period 200 seconds							
Only 8 grams of chrome alum in pill							
Demagnetization. Search coil deflection +3 cm.							
17:08	200 sec.	9298	29261	.927	1.017	(8.8±1.2)	.044±.005 ^{+.007}
	"	9460	29092				
	"	9332	28830	.923	1.007	8.4±1.2	.045
	"	9329	28917				
Swept remnant field deflection = -.3 cm.							
	200 sec.	9580	29309	.958	1.020	6.1±1.2	.053
:27	"	9571	29162				
	"	9493	29363	.947	1.027	7.8±1.2	.045
	"	9668	29522				
:40	"	9617	29313	.966	1.017	5.0±1.2	.056

Time	Counting Period	Raw* Counts Axial	Raw* Counts Equa- torial	Normalized (0) Axial	Normalized (90°) Equa- torial	ε %	T (K)
	200 sec.	9824	28883				
	"	9621	29083	.967	1.015	4.7±1.2	.059±.007
:51	"	9930	29107				
Normalization							
	4 x 200 sec.*	10113	28676				



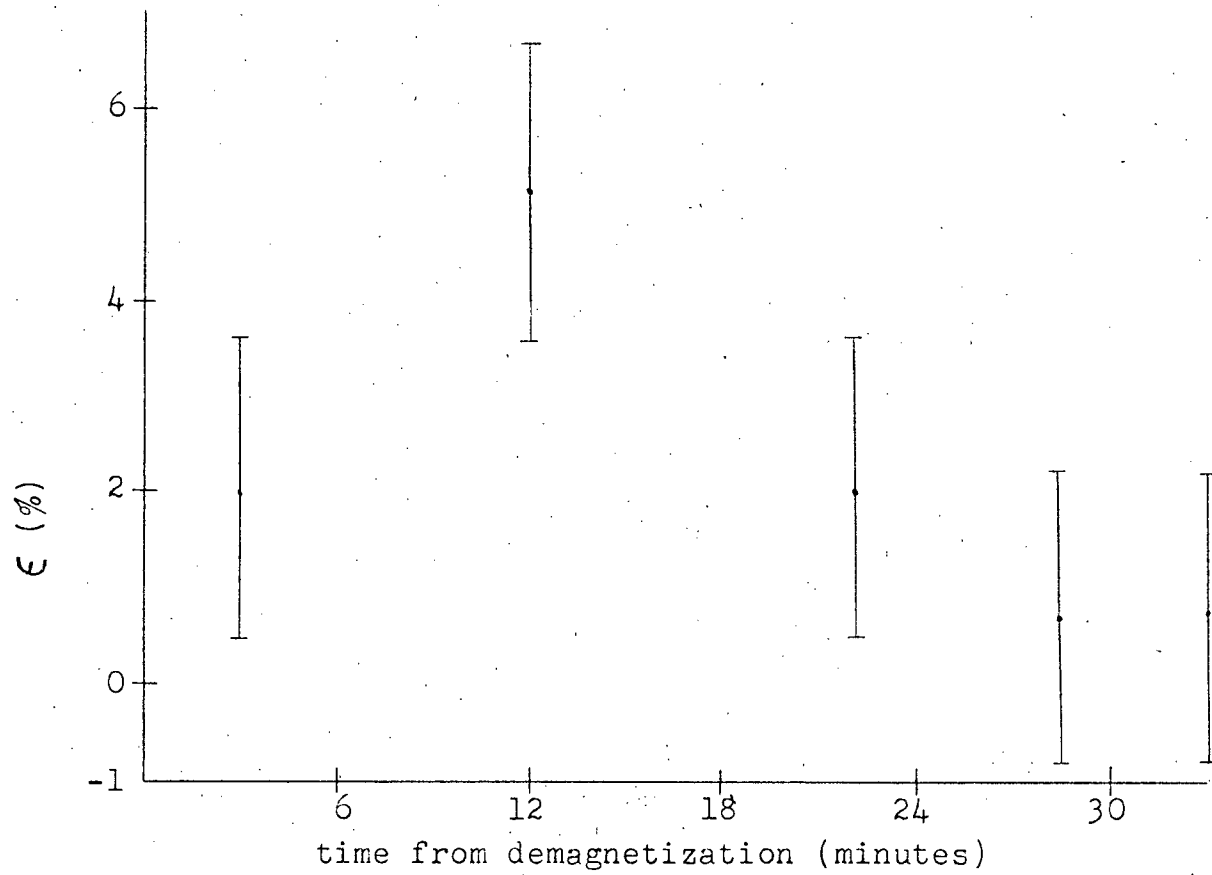
Run 1

FIGURE 3.4



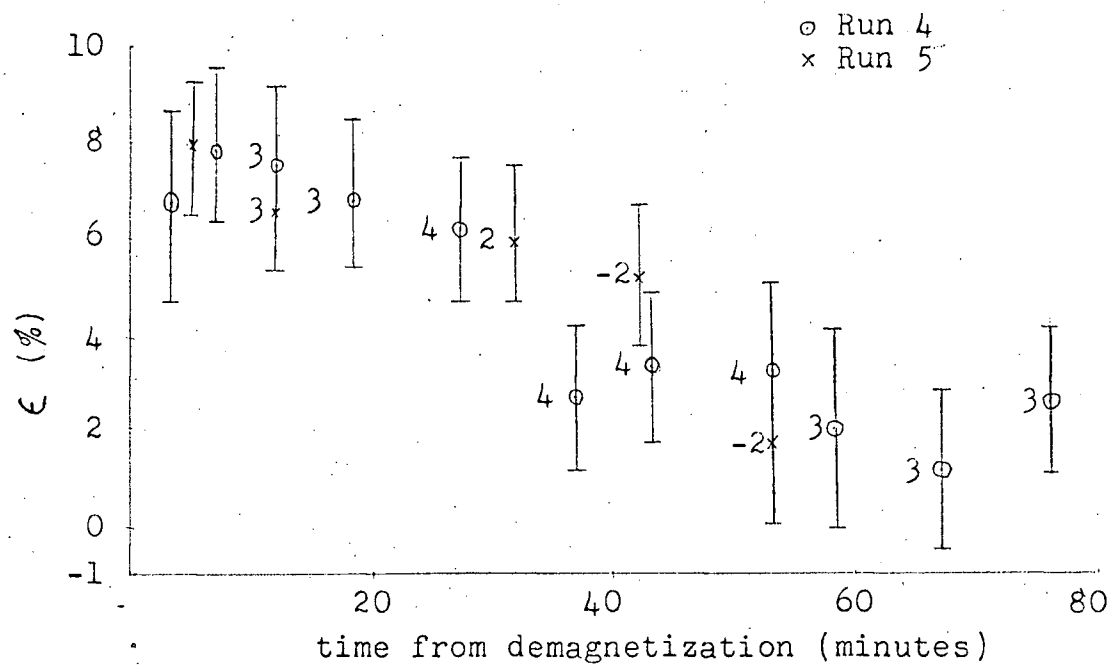
Run 2

FIGURE 3.5



Run 3 - An Uninterrupted Run

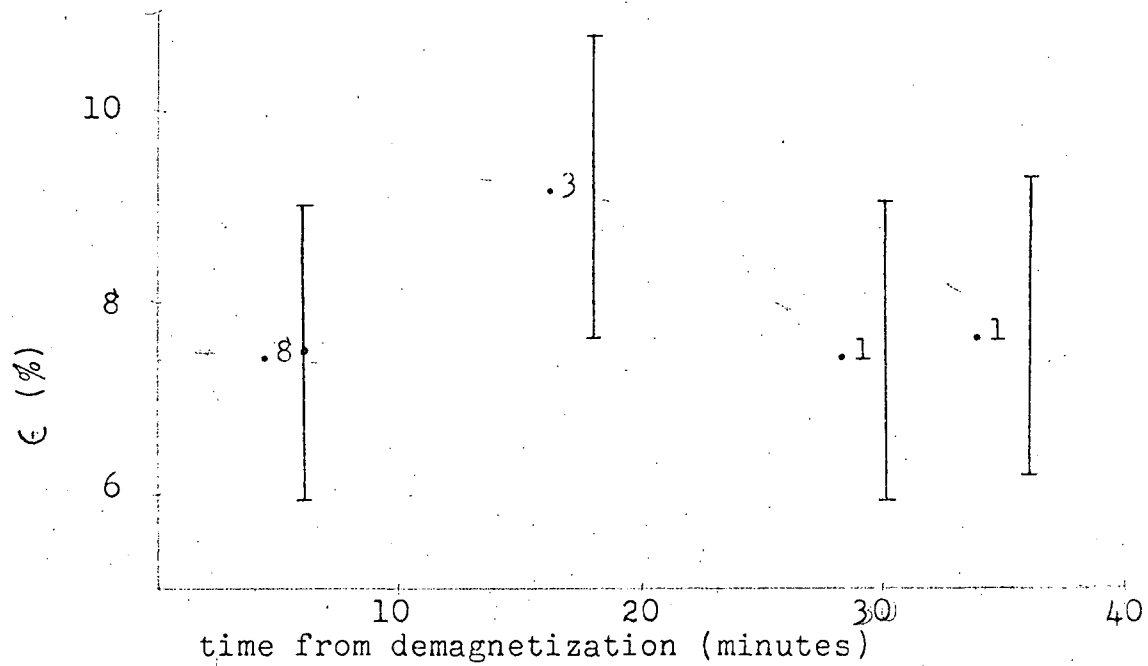
FIGURE 3.6



The current, in amperes, in the polarizing coil prior to the reading is given beside each data point.

Runs 4 and 5

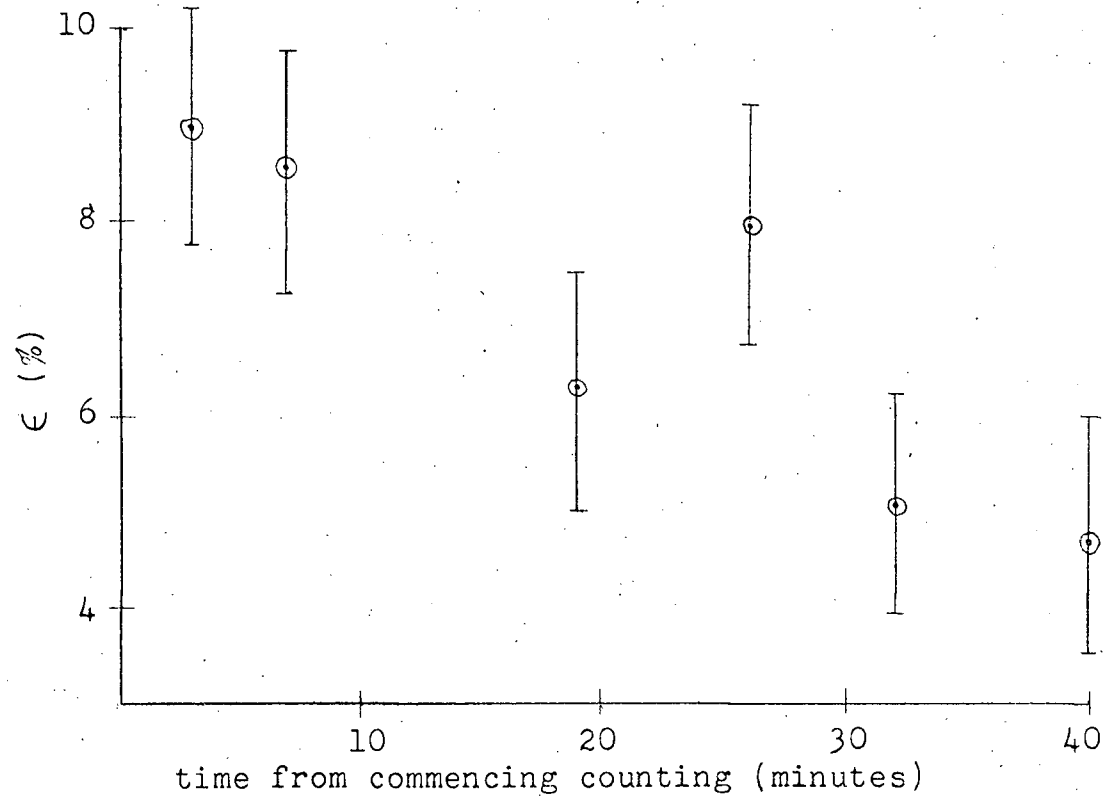
FIGURE 3.7



The residual field measurements (deflections in cm.) are given beside each data point.

Run 6

FIGURE 3.8



Note. In this run there were only eight grams of chrome alum in the pill.

Run 7

FIGURE 3.9

The sources of possible heat leaks and the effects of magnetic fields which cause high temperature at the specimen source have been discussed in this work. If the heating were due solely to a heat leak it would have to be about 40 erg/sec. On the other hand, if only 10% of the heat link is in good contact with the alum the same results occur. At the present time the reason for the relatively high final temperature is not known. Some improvements in the apparatus will have to be made before original experimental work can be carried out. Many such changes are currently being attempted including the construction of a new apparatus described in Chapter IV.

CHAPTER IV

FUTURE MODIFICATIONS OF THE APPARATUS

A new apparatus is being constructed. It is hoped to remove some of the limitations of the present low temperature system. In addition some changes in technique are being considered such as resonant destruction of nuclear orientation and detection of beta radiations. Furthermore, modifications are being made to the present low temperature apparatus.

4.1 Low Temperature

i) Heat Leaks to the Demagnetized System The heat leak by gas conductivity and absorption of exchange gas will be reduced by shielding the chrome alum pill by a sleeve thermally anchored to the guard pill. Also use of a metal high-vacuum system will reduce the (partial) pressure of helium in the system. The metal system requires no vacuum grease seals in the inner jacket line which reduces the outgassing of helium. Furthermore, it can be readily heated to reduce outgassing. The pumping lines will be larger in diameter to give higher pumping speed if required.

The new support framework will be rigidly mounted at the base in a concrete block supported by steel springs. This will increase the rigidity thereby reducing the vibrational heat leak. Furthermore, all pumping lines to the cryostat can be firmly secured outside the cryostat to keep out pump vibrations. The springs under the system damp out vibrations from the floor.

The chrome alum pill will be made larger. This will allow the use of more chrome alum to lengthen the "cold time". Also more wires can be

used in the heat link to increase the contact area.

ii) The Remnant Field The new system has been designed to allow the demagnetization solenoid to be raised above the chrome alum. This will completely remove the remnant field. If cerium magnesium nitrate were used for demagnetizations to lower temperatures such removal of the field could be important.

iii) The 1 K Helium Bath The double walled helium bath presently being used will be changed. Instead, an enclosed can of liquid helium at the top of the inner jacket will be used. The jacket will be made of copper to ensure good thermal conductivity. The volume of the can will be about 150 cc. which will hold more liquid than the present system so that refilling will not be necessary. The use of a single jacket leaves more room in the demagnetization chamber. This allows the shielding of the pill and the increase in size of the pill. Furthermore, the inner cryostat will be lengthened to allow a larger pill and to further separate the pill from the polarizing solenoid. Larger pumping lines in the inner cryostat will increase the pumping speed and reduce the bath pressure and temperature.

iv) Liquid Helium Loss A liquid nitrogen pot at the top of the pumping lines will reduce the heat leak into the 4 K helium reservoir. The leads to the superconducting solenoid will be in thermal contact with the liquid nitrogen. This should reduce the helium loss rate by a factor of at least two.

4.2 Resonant Destruction of Nuclear Orientation

Resonant destruction of nuclear orientation was discussed in section 1.7. The new apparatus will be suitable for resonant experiments. A

small radio frequency coil will be wound in the demagnetization chamber around the source with its axis perpendicular to the axis of quantization. The r.f. power input to the source must be kept small to prevent heating.

4.3 Detectors

i) Ge(Li) Detectors Lithium drifted germanium solid state gamma detectors have far greater resolution than the sodium iodide scintillation counters. This allows easier separation of gamma ray contributions in the radiation spectrum. However, the low efficiency of the devices require stronger sources and longer counting times to keep the statistical error low.

ii) Si(Li) Detectors Lithium drifted silicon solid state detectors are used to detect beta radiation. Because the beta rays are completely attenuated by the cryostat, the detector must be placed inside the demagnetization chamber. However, the detectors have proved to be very temperature sensitive and a device for warming the detector above the bath temperature may be necessary.

REFERENCES

- 1 M. E. Rose, Elementary Theory of Angular Momentum, 179 (John Wiley and Sons, Inc., New York, 1967).
- 2 T. P. Gray and G. R. Satchler, Proc. Phys. Soc., London, A68, 349, (1955).
- 3 R. J. Blin-Stoyle and M. A. Grace, Handbuch der Physik 42, 555 (Springer, Berlin, 1957).
- 4 S. R. De Groot, H. A. Tolhoek, and W. J. Huiskamp, Alpha-, Beta-, and Gamma-Ray Spectroscopy, Vol. 2, p. 1199 (Kai Siegbahn, editor, North Holland, Amsterdam, 1965).
- 5 B. Bleaney, Hyperfine Interactions (A. J. Freeman, R. B. Frandel, editors, Academic Press, New York, 1965).
- 6 W. A. Little, Can. J. Phys. 37, 334 (1959).
- 7 A. C. Anderson, G. L. Salinger, J. C. Wheatley, Rev. Sci. Instr., 32, p. 1110 (1961).
- 8 A. J. Freeman, R. E. Watson, Treatise on Magnetism, Vol. IIA (Suhl-Rado, editors, Academic Press, New York, 1965).
- 9 V. L. Sedov, L. V. Golomatina and L. A. Kondrashova, Soviet Physics JETP, 27, p. 870 (1968).
- 10 E. Daniel, op. cit., reference 5.
- 11 D. A. Shirley, S. S. Rosenblum, and E. Matthias, Phys. Rev. 170, p. 363 (1968).
- 12 A. E. Balabanov and N. N. Delyagin, Soviet Physics JETP, 27, p. 752 (1968).
- 13 A. J. Freeman, Hyperfine Structure and Nuclear Radiations, (E. Matthias and D. A. Shirley, editors, North-Holland Publishing Co., Amsterdam, 1968).
- 14 J. E. Templeton and D. A. Shirley, Phys. Rev. Letters, 18, p. 240 (1967).
- 15 A. C. Anderson, W. R. Roach and R. E. Sarwinski, Rev. Sci. Instr., 37, p. 1024 (1961).
- 16 G. K. White, Experimental Techniques in Low Temperature Physics, p. 179 (Oxford, 1959).
- 17 V. S. Shirley, Table of Nuclear Moments, op. cit., reference 13.
- 18 Y. Koi, A. Tsujimura, J. Phys. Soc., Japan, 16, p. 1040 (1961).
- 19 M. L. Rose, Phys. Rev. 91, p. 610 (1963).
- 20 B. G. Turrell, D. Phil. Thesis (University of Oxford, unpublished, 1963).